TRIP13 localizes to synapsed chromosomes and functions as a dosage-sensitive regulator of meiosis

Jessica Y. Chotiner[1], N. Adrian Leu[1], Fang Yang[1], Isabella G. Cossu[1], Yongjuan Guan[1,2], Huijuan Lin[1], and P. Jeremy Wang[1],*

[1]Department of Biomedical Sciences, University of Pennsylvania School of Veterinary Medicine, Philadelphia, PA 19104, USA. [2]College of Life Sciences, Capital Normal University, Beijing, China.

*For correspondence: pwang@vet.upenn.edu

Abstract

Meiotic progression requires coordinated assembly and disassembly of protein complexes involved in chromosome synapsis and meiotic recombination. The AAA+ ATPase TRIP13 and its orthologue Pch2 are instrumental in remodeling HORMA domain proteins. Meiosis-specific HORMAD proteins are associated with unsynapsed chromosome axes but depleted from the synaptonemal complex (SC) of synapsed chromosome homologues. Here we report that TRIP13 localizes to the synapsed SC in early pachytene spermatocytes and to telomeres throughout meiotic prophase I. Loss of TRIP13 leads to meiotic arrest and thus sterility in both sexes. *Trip13*-null meiocytes exhibit abnormal persistence of HORMAD1 and HOMRAD2 on synapsed SC and chromosome asynapsis that preferentially affects XY and centromeric ends. These findings confirm the previously reported phenotypes of the *Trip13* hypomorph alleles. *Trip13* heterozygous (*Trip13*$^{+/-}$) mice also exhibit meiotic defects that are less severe than the *Trip13*-null mice, showing that TRIP13 is a dosage-sensitive regulator of meiosis. Localization of TRIP13 to the synapsed SC is independent of SC axial element proteins such as REC8 and SYCP2/SYCP3. The N- or C-terminal FLAG-tagged TRIP13 proteins are functional and recapitulate the localization of native TRIP13 to SC and telomeres in knockin mice. Therefore, the evolutionarily conserved localization of TRIP13/Pch2 to the synapsed chromosomes provides an explanation for dissociation of HORMA domain proteins upon chromosome synapsis in diverse organisms.

Introduction

Meiosis is a specialized cell division program that generates haploid gametes from diploid germ cells. During meiotic prophase I, homologous chromosomes undergo paring, synapsis, and recombination (Handel and Schimenti, 2010; Zickler and Kleckner, 2015). Chromosome synapsis requires the formation of the synaptonemal complex (SC). The SC is a proteinaceous structure comprised of two lateral/axial elements, transverse filaments, and a central element (Page and Hawley, 2004). Meiotic recombination begins with generation of DNA double strand breaks (DSBs) and ends with crossover formation through repair of DSBs (Hunter, 2015). Chromosome synapsis and meiotic recombination are interdependent in many species including yeast and mouse. Meiotic recombination not only increases genetic diversity in gametes at the organism level but also is essential for faithful chromosome segregation during the first meiotic cell division. Therefore, defects in meiosis are leading causes of aneuploidy, birth defect, infertility, and pregnancy loss.

The progression and completion of synapsis and recombination are monitored by a surveillance mechanism called meiotic checkpoint (Roeder and Bailis, 2000). Meiotic checkpoint proteins were extensively studied in yeast. Many meiotic processes are highly conserved, and studies of meiosis in yeast

46 have been foundational for our understanding of mammalian meiosis. In yeast, Pch2, an AAA+ ATPase,
47 is a checkpoint protein, because it is necessary for pachytene arrest in the absence of the SC protein Zip1
48 or the meiosis-specific DSB repair protein Dmc1 (Herruzo et al., 2021; San-Segundo and Roeder, 1999).
49 Pch2 is a hexameric ring ATPase and remodels the HORMA (Hop1, Rev7, and MAD2) domain protein
50 Hop1 in a nucleotide-dependent manner (Chen et al., 2014). While Pch2 is mainly located in the
51 nucleolus, Pch2 also localizes to the synapsed SC as foci at the pachytene stage and is essential for
52 removing Hop1 from chromosome axes (Chen et al., 2014; Joshi et al., 2009; San-Segundo and Roeder,
53 1999). Mechanistically, Pch2 promotes phosphorylation of Hop1, which activates the Mek1 kinase and
54 the subsequent checkpoint cascade (Herruzo et al., 2016; Raina and Vader, 2020).
55 TRIP13, the mammalian orthologue of yeast Pch2, is essential for completion of meiotic
56 recombination in mouse (Li and Schimenti, 2007; Roig et al., 2010). Mutations in human *TRIP13*
57 predispose to Wilms tumor in children or cause infertility in women (Yost et al., 2017; Zhang et al.,
58 2020). HORMAD1 and HORMAD2, mammalian meiosis-specific HORMA domain proteins, localize to
59 chromosome axis at leptotene and zygotene stages but are depleted from synapsed chromosomes except
60 the largely unsynapsed XY chromosomes at the pachytene stage (Fukuda et al., 2010; Xu et al., 2019).
61 TRIP13 facilitates removal of HORMAD proteins from synapsed chromosome axis (Roig et al., 2010;
62 Wojtasz et al., 2009). SKP1, an essential component of the SCF (Skp1-Cullin 1-F-box protein) ubiquitin
63 E3 ligase, is required not only for depleting HORMAD1 and HORMAD2 from synapsed chromosome
64 axes but also for restricting the accumulation of HORMAD proteins on unsynapsed axes (Guan et al.,
65 2020; Guan et al., 2022). Therefore, reorganization of HORMA domain proteins on meiotic chromosome
66 axes is regulated by both TRIP13 and SKP1. As a conserved mechanism, Pch2/TRIP13 remodels
67 HORMA domain proteins through engagement of their N-terminal regions (Prince and Martinez-Perez,
68 2022). MAD2, a spindle assembly checkpoint HORMA domain protein, exists in two fold states: closed
69 and open (Luo et al., 2004; Sironi et al., 2002). In the closed state, the so-called safety belt of the
70 HORMA domain wraps around the HORMAD protein-binding motif "closure motif" in the partner
71 protein and thus traps the partner. In the open state, TRIP13 engagement changes conformation of the
72 HORMA domain, resulting in foldback of the safety belt on the closure motif-binding region and thus
73 release of its partner protein. The safety belt mechanism turns out to be a shared feature of HORMA
74 domain proteins (Kim et al., 2014; West et al., 2019; West et al., 2018; Ye et al., 2017).
75 Unlike yeast Pch2, TRIP13 does not appear to function in the meiotic checkpoint in mouse
76 (Pacheco et al., 2015). Interestingly, HORMAD2 functions as a meiotic checkpoint protein for
77 surveillance of meiotic defects in female meiosis (Kogo et al., 2012a; Rinaldi et al., 2017; Wojtasz et al.,
78 2012). HORMAD2-deficient males are sterile but females are fertile. HORMAD2 deficiency rescues the

79 oocyte loss in *Spo11*-null or *Trip13* mutant females but not in *Dmc1*-null females, suggesting that
80 HORMAD2 is a component of the meiotic checkpoint in females. HORMAD1 is required for fertility in
81 both sexes (Kogo et al., 2012b; Shin et al., 2010; Stanzione et al., 2016). Both HORMAD1 and
82 HORMAD2 localize prominently to the XY chromosome axes in pachytene spermatocytes and regulate
83 meiotic sex chromatin inactivation (MSCI) (Kogo et al., 2012a; Shin et al., 2010; Wojtasz et al., 2012).
84 Studies of mice with hypomorphic *Trip13* mutations show that TRIP13 is required for meiotic
85 progression (Li and Schimenti, 2007; Roig et al., 2010). Two different hypomorphic *Trip13* mouse lines
86 have been studied: one "moderate" allele that exhibited defective meiotic recombination and one "severe"
87 allele that displayed defects in meiotic recombination and chromosome synapsis. The variance in
88 phenotype between the hypomorphic mouse lines indicates that even partial depletion of *Trip13* can
89 interrupt meiosis. We sought to further investigate the meiotic function of TRIP13. By
90 immunofluorescence, we found that TRIP13 localized to the synaptonemal complex in early pachytene
91 spermatocytes and to telomeres throughout meiotic prophase I. The TRIP13 localization pattern on
92 meiotic chromosomes was further confirmed by analysis of FLAG-tagged TRIP13 in two knockin mouse
93 lines. To determine the effect of complete loss of TRIP13, we characterized *Trip13*-null mice. While the
94 *Trip13*-null phenotype was largely comparable to the phenotype of the severe *Trip13* hypomorphic allele,
95 we found that TRIP13 is a dosage-sensitive regulator of meiosis. Finally, our results show that the
96 localization of TRIP13 to the SC is independent of axial element proteins.
97
98 **Results**
99
100 **TRIP13 localizes to meiotic chromosomes in prophase I spermatocytes**
101 We assessed the expression of TRIP13 in a panel of adult mouse tissues. TRIP13 was primarily expressed
102 in testis but detected at low levels in ovary and liver (Figure 1A). In the testis, TRIP13 was prominent in
103 the cytoplasm of primary spermatocytes, especially leptotene and zygotene cells (Figure 1B). Given the
104 expression of TRIP13 in spermatocytes, we examined its localization on meiotic chromosomes by
105 immunostaining of surface spread nuclei of prophase I spermatocytes (Figure 1C). Previously, TRIP13
106 was reported to localize to telomeres in spermatocytes (Gomez et al., 2019). Indeed, we found that
107 TRIP13 localized to telomeres from leptotene to diplotene cells (Figure 1C). Strikingly, we found that, in
108 addition to telomeres, TRIP13 localized to the synaptonemal complex (SC) in early pachytene
109 spermatocytes but disappeared from the SC in the mid to late pachytene spermatocytes (Figure 1C). The
110 synaptonemal complex consists of two lateral elements and one central element. The central region is
111 comprised of the transverse filament protein SYCP1 and central element proteins, which appear upon

synapsis. Given the novel localization of TRIP13 to the SC, we performed confocal immunofluorescent microscopy with super-resolution deconvolution to determine the location of TRIP13 within the SC. In contrast with the lateral element marker SYCP3, TRIP13 localized to the SC central region (Figure 1D). We examined the localization of TRIP13 in oocytes. TRIP13 localized strongly to meiotic telomeres in all stages of prophase I, but not as filaments on the SC (Figure 1 - figure supplement 1). These findings are consistent with the genetic requirement of TRIP13 in meiosis in both sexes (Li and Schimenti, 2007; Roig et al., 2010).

Global loss of *Trip13* causes meiotic arrest

Two previous studies utilizing two *Trip13* hypomorphic (gene trap) alleles, one moderate and one severe, revealed a role for TRIP13 in meiotic recombination (Li and Schimenti, 2007; Roig et al., 2010). However, while the *Trip13* moderate allele showed mostly intact chromosomal synapsis, the severe allele displayed chromosomal unsynapsis preferentially at chromosome ends (Li and Schimenti, 2007; Roig et al., 2010). Upon close examination, we also found unsynapsed ends in spermatocytes with the moderate *Trip13* mutant (Guan et al., 2020). To rigorously ascertain the role of TRIP13 in meiosis, we generated *Trip13*-null mutants using frozen sperm from *Trip13*$^{+/-}$ males with a knockout allele from the International Mouse Phenotyping Consortium (IMPC). The mouse *Trip13* gene consists of 13 exons. This new *Trip13* mutant allele harbors a deletion of a 24-kb region including all 13 exons and thus is expected to be null. We verified this deletion by PCR and sequencing. Interbreeding of *Trip13*$^{+/-}$ mice produced fewer *Trip13*$^{-/-}$ offspring than expected: *Trip13*$^{+/+}$, 80; *Trip13*$^{+/-}$, 220; *Trip13*$^{-/-}$, 51 ($\chi 2=27$, $p=0.0001$). The body weight of 2-3 month-old males was not significantly different between wild type (24.3±2.8 g, n=5) and *Trip13*$^{-/-}$ mice (22.8±1.7 g, n=5, $p=0.3$, Student's *t*-Test). The *Trip13*$^{-/-}$ testis was much smaller than *Trip13*$^{+/-}$ testis (Figure 2A). Western blot analysis showed that TRIP13 was present in reduced abundance in *Trip13*$^{+/-}$ testis and not detected in *Trip13*$^{-/-}$ testis, demonstrating that this mutant allele is null (Figure 2B). The abundance of SYCP3, a component of the synaptonemal complex, was also reduced in *Trip13*$^{-/-}$ testis, suggesting a partial depletion of meiotic cells (Figure 2B). The testis weight of adult *Trip13*$^{-/-}$ males was reduced by 74% in comparison with the wild type males (Figure 2C). Adult *Trip13*$^{-/-}$ males lacked sperm in the epididymis (Figure 2D). Histological analysis showed that while spermatocytes in all stages of meiosis were present in adult *Trip13*$^{+/+}$ and *Trip13*$^{+/-}$ testes, *Trip13*$^{-/-}$ testis displayed complete meiotic arrest, evidenced by the presence of early spermatocytes and a lack of secondary spermatocytes, round spermatids, and mature sperm (Figure 2E). *Trip13*$^{-/-}$ females were also sterile. The adult *Trip13*$^{-/-}$ ovary was very small and showed a complete loss of oocytes (Figure 2 - figure supplement 1). These

144 observations are similar to the meiotic arrest phenotype observed in the hypomorphic *Trip13* mouse
145 mutants (Li and Schimenti, 2007; Roig et al., 2010).
146
147 **Defects in chromosomal synapsis in *Trip13*-deficient spermatocytes**
148 We investigated the effect of *Trip13* deficiency on meiotic progression. The transverse filament/central
149 element protein SYCP1 and the lateral element protein SYCP3 were used to determine the stage of
150 prophase I spermatocytes. While the P20 wild type testis contained spermatocytes from leptotene through
151 diplotene stages, about half of the *Trip13*$^{-/-}$ spermatocytes were in the early pachytene stage and no cells
152 were found at later stages of prophase I, showing meiotic blockade at the early pachytene stage in *Trip13*$^{-}$
153 $^{/-}$ testes (Figure 3A). The early pachytene-like spermatocytes from *Trip13*$^{-/-}$ testes contained unsynapsed
154 chromosomal ends (Figure 3B). Mouse centromeres are telocentric. Co-staining with the centromere
155 marker CREST showed that 94% of unsynapsed ends were centromeric ends (Figure 4A). While XY
156 chromosomes were synapsed at the pseudoautosomal regions and thus were connected in wild type and
157 *Trip13*$^{+/-}$ pachytene spermatocytes, they were separate in *Trip13*$^{-/-}$ pachytene-like spermatocytes (Figure
158 3B and Figure 3C). We found that SYCE1, a component of the SC central element, localized to the
159 synapsed SC but not to unsynapsed regions in *Trip13*$^{-/-}$ pachytene-like cells (Figure 3C). Confocal
160 microscopy with super-resolution deconvolution confirmed that many homologous chromosomes in
161 *Trip13*$^{-/-}$ spermatocytes had split ends and some had regions of interstitial asynapsis (Figure 3D). We
162 quantified these meiotic defects in spermatocytes: chromosomal asynapsis (Figure 3E), the number of
163 asynapsed ends (Figure 3F), and the extent of XY asynapsis (Figure 3G). Previous studies also reported
164 synaptic defects in spermatocytes from *Trip13* hypomorph mutants (Li and Schimenti, 2007; Roig et al.,
165 2010). Here we found that global loss of *Trip13* caused similar defects in autosomal synapsis but a more
166 severe defect in sex chromosome synapsis.
167
168 **TRIP13 is a dosage-sensitive regulator of meiosis**
169 Although *Trip13*$^{+/-}$ males were fertile, their testis weight and sperm count were significantly reduced in
170 comparison with wild type (Figure 2C-D). The percentage of spermatocytes with defects in synapsis was
171 higher in *Trip13*$^{+/-}$ males than wild type (Figure 3E). In addition, the percentage of spermatocytes with
172 asynapsed XY chromosomes was significantly higher in *Trip13*$^{+/-}$ males than wild type (Figure 3G). As
173 defects in synapsis can activate the meiotic checkpoint and thus apoptosis of affected spermatocytes, the
174 increased synaptic defects likely caused the decrease in sperm output in *Trip13*$^{+/-}$ males. These results
175 demonstrate that TRIP13 regulates meiosis in a dosage-dependent manner.
176

177 **Telomere and centromere proteins localize normally in *Trip13*-deficient spermatocytes**
178 TRIP13 localizes to telomeres and loss of TRIP13 causes peri-centromeric/telomeric asynapsis.
179 Therefore, we asked whether telomere or centromere proteins were affected in *Trip13*$^{-/-}$ spermatocytes.
180 Chromosome spreads were immunostained for two centromere markers, CREST and CENPC (Figure 4A-
181 B). CENPC is essential for recruiting kinetochore proteins to the centromere (Klare et al., 2015; Kwon et
182 al., 2007). CREST and CENPC still localized to centromeres in *Trip13*$^{-/-}$ spermatocytes. Because many
183 *Trip13*$^{-/-}$ spermatocytes had split ends, two CREST or two CENPC foci were observed at the split ends.
184 To assess the telomere, spermatocytes were immunostained for TRF1 and MAJIN (Figure 4C-D). In
185 meiotic cells, telomeres contain canonical telomere proteins such as TRF1/TRF2 and a meiosis-specific
186 complex (MAJIN, TERB1, TERB2, and SUN1) (Shibuya et al., 2015). TRF1 is a telomere protein
187 expressed in both somatic and germ cells (Karlseder et al., 2003; Long et al., 2017; Shibuya et al., 2014).
188 MAJIN is a component of the meiosis-specific telomere complex that is important for telomere
189 attachment to the inner nuclear membrane (Shibuya et al., 2015). Both TRF1 and MAJIN localized to
190 telomeres in *Trip13*$^{-/-}$ spermatocytes (Figure 4C-D). As expected, two TRF1 or two MAJIN foci were
191 observed at split ends of chromosomes in *Trip13*$^{-/-}$ spermatocytes (Figure 4C-D). ANKRD31 and REC114
192 interact with each other and both localize to the pseudoautosomal region (PAR) of XY chromosomes in
193 early pachytene spermatocytes to ensure XY recombination (Boekhout et al., 2019; Papanikos et al.,
194 2019). In addition to two foci on autosomes, REC114 localized as one focus on the PAR in wild type
195 pachytene spermatocytes. REC114 still formed foci (one per chromosome) on the unsynapsed X and Y
196 chromosomes in *Trip13*$^{-/-}$ pachytene-like spermatocytes (Figure 4 - figure supplement 1). Taken together,
197 these results suggest that TRIP13 is not required for recruitment of these centromere or telomere proteins.
198
199 **TRIP13 is required to evict HORMAD1 and HORMAD2 from synapsed autosomes**
200 In wild type meiotic cells, HORMAD1 and HORMAD2 localize to unsynapsed and desynapsed
201 chromosomes (Fukuda et al., 2010; Kogo et al., 2012a; Shin et al., 2010; Wojtasz et al., 2012). Thus,
202 HORMAD1 and HORMAD2 localized to the largely unsynapsed XY but not to synapsed autosomal SCs
203 in wild type cells (Figure 5A-B). TRIP13 is essential for removing meiotic HORMADs from the
204 chromosome axes, a function that is conserved in yeast, worms, and mammals (Wojtasz et al., 2009). We
205 confirmed that HORMAD1 and HORMAD2 remained on the synapsed autosomes in *Trip13*$^{-/-}$ pachytene
206 cells (Figure 5A-B). HORMAD1 and HORMAD2 localize to the interior of the lateral elements in the SC
207 (Xu et al., 2019). Confocal microscopy with super-resolution deconvolution revealed that HORMAD1
208 and HORMAD2 localized to the lateral elements of the synapsed autosomes in *Trip13*$^{-/-}$ spermatocytes
209 (Figure 5C-D). These results were consistent with accumulation of HORMAD1/2 in *Trip13* hypomorphic

210 mutant spermatocytes (Roig et al., 2010; Wojtasz et al., 2009). Our analysis of *Trip13*-null mutant
211 confirmed that TRIP13 is essential for HORMAD1/2 removal from the synapsed SCs.
212
213 **Localization of TRIP13 to SC is independent of axial element components**
214 TRIP13 localizes to the SC in early pachytene spermatocytes. We sought to address what proteins might
215 recruit TRIP13 to the SC. We examined the role of HORMAD1, REC8, SYCP2, and SKP1 in TRIP13
216 localization in spermatocytes using respective knockout mice (Figure 6). We first examined the
217 localization of TRIP13 in *Hormad1*$^{-/-}$ spermatocytes. *Hormad1*$^{-/-}$ spermatocytes exhibit limited synapsis
218 (Daniel et al., 2011; Kogo et al., 2012b; Shin et al., 2010). In both wild type and *Hormad1*$^{-/-}$ cells, TRIP13
219 localized to the synapsed regions and to the telomeres (Figure 6A). This result shows that HORMAD1 is
220 not required for localization of TRIP13 to the SC.
221 REC8, a meiosis-specific cohesin, promotes synapsis between homologs and inhibits synapsis
222 between sister chromatids (Xu et al., 2005). In the absence of REC8, synapsis occurs between sister
223 chromatids rather than homologous chromosomes as previously shown by super-resolution imaging
224 (Guan et al., 2020). In *Rec8*$^{-/-}$ spermatocytes, TRIP13 localized to synapsed sister chromatids (Figure 6B).
225 To further probe TRIP13 recruitment to the SC, a mouse line expressing a truncated SYCP2 was used
226 (Yang et al., 2006). SYCP2 and SYCP3 are essential components of the axial/lateral elements of the SC
227 and interact with each other. The mutant used in this study (referred to as *Sycp2*$^{-/-}$) expresses a truncated
228 SYCP2 protein that lacks the C-terminal coiled-coil domain necessary for binding to SYCP3. Thus,
229 SYCP3 failed to localize to the axial elements and formed aggregates in *Sycp2*$^{-/-}$ spermatocytes (Figure
230 6C). Nevertheless, *Sycp2*$^{-/-}$ spermatocytes formed short stretches of synapsis as previously demonstrated
231 by electron microcopy and SYCP1 immunofluorescence (Yang et al., 2006). TRIP13 localized as
232 filaments in *Sycp2*$^{-/-}$ spermatocytes, strongly suggesting that its localization is independent of SYCP3 and
233 the C-terminus of SYCP2 (Figure 6C).
234 Previous work has shown that SKP1, a key component of the SKP1, Cullin, F-box (SCF) complex
235 E3 ligase, is important for HORMAD removal and chromosomal synapsis (Guan et al., 2020; Guan et al.,
236 2022). SKP1 localizes to synapsed regions in meiotic germ cells and specifically to the lateral elements in
237 the SC (Guan et al., 2020). We found that TRIP13 still localized to the synapsed regions in *Skp1*^{cKO}
238 (conditional knockout) spermatocytes (Figure 6D). Taken together, these results show that the SC
239 localization of TRIP13 is independent of HORMAD1, REC8, SYCP2, SYCP3, and SKP1, which all
240 localize to the SC lateral elements. Such a finding is consistent with the localization of TRIP13 to the SC
241 central region (Figure 1D).
242

243 **FLAG-tagged TRIP13 proteins are functional**

244 In order to investigate the mechanism of TRIP13 recruitment to the SC, we generated 3×FLAG-TRIP13
245 (N-terminal tag) and TRIP13-3×FLAG (C-terminal tag) mice through the CRISPR/Cas9-medidated
246 genome editing approach (Figure 7 - figure supplement 1). Two different types of tagged mice were
247 generated in case that one fusion protein is not functional. Both alleles were transmitted through the
248 germline of the founder mice. Western blot showed that TRIP13 existed in two isoforms in wild type
249 (non-tagged) testis (Figure 7A). The major TRIP13 isoform was 50 kDa. The minor isoform was slightly
250 larger than 50 kDa. Western blot analysis showed that the FLAG tagged TRIP13 fusion proteins were
251 present in both FLAG-tagged testes. Both FLAG-tagged TRIP13 fusion proteins also existed in two
252 isoforms in the homozygous testes, suggesting that they corresponded to the two wild type isoforms. The
253 3×FLAG-TRIP13 proteins were apparently slightly larger, possibly due to the linker in the N-terminally
254 tagged proteins. The nature and physiological significance of these two isoforms were not clear, but could
255 be due to alternative splicing or post-translational modification. Immunofluorescence analysis using anti-
256 FLAG antibody showed that the FLAG-tagged TRIP13 proteins, like wild type TRIP13, localized to both
257 telomeres and synaptonemal complex in pachytene spermatocytes from both FLAG/FLAG homozygous
258 testes (Figure 7B). Importantly, both N- and C-terminally tagged homozygous mice were fertile. These
259 results demonstrate that both N- and C-terminal tagged TRIP13 proteins localize normally and are
260 functional.

261 To identify TRIP13-associated proteins in testis, we performed immunoprecipitation (IP) using
262 3×FLAG-TRIP13, TRIP13-3×FLAG, and wild type (no tag) testicular protein extracts with anti-FLAG
263 monoclonal antibody. The immunoprecipitated proteins were eluted with FLAG peptides and subjected to
264 mass spectrometry for protein identification. As expected, TRIP13 had more peptides in tagged TRIP13
265 IP than wild type (Table 1). HORMAD2, a known TRIP13 substrate protein, was also enriched in tagged
266 TRIP13 IP (Table 1). Intriguingly, a large number of RNA-binding proteins involved in RNA splicing
267 were highly enriched in tagged TRIP13 IP: DDX46, PUF60, RBM25, RBM39, U2AF1, U2AF2, and
268 SRSF11 (Table 1). The biological relevance of these RNA-binding proteins to TRIP13 function remains
269 unknown. We cannot exclude the possibility that identification of these RNA splicing factors could be
270 immunoprecipitation artifacts.

271

272 **Discussion**

273 TRIP13 and its orthologue Pch2 play an evolutionarily conserved role in depletion of meiosis-specific
274 HORMA domain proteins from the synaptonemal complex in many species including yeast, plant, and
275 mouse. In meiocytes, HORMA domain proteins are associated with unsynapsed chromosome axes and

276 become depleted from the SC upon synapsis (Figure 7C). In mice with *Trip13* hypomorphic gene trap
277 alleles, HORMAD1 and HORMAD2 persist on the synapsed SCs at the pachytene stage (Wojtasz et al.,
278 2009). In this study, we confirmed the abnormal persistence of HORMAD1 and HORMAD2 in *Trip13*-
279 null spermatocytes (Figure 7C). In budding yeast, deficiency of Pch2 leads to accumulation of Hop1 on
280 the SC (Joshi et al., 2009; Subramanian et al., 2016). In *Arabidopsis*, Pch2 remodels the HORMA domain
281 protein ASY1 (Balboni et al., 2020; Yang et al., 2020). Pch2 has been shown to localize to synapsed SC
282 in budding yeast (Joshi et al., 2009), C. elegans (Deshong et al., 2014; Russo et al., 2023), *Arabidopsis*
283 (Lambing et al., 2015), and rice (Miao et al., 2013), but not in mice. In mouse meiocytes, TRIP13 was
284 known to localize to telomeres (Gomez et al., 2019). In addition to telomeres, we find that TRIP13
285 localizes to the SC in early pachytene spermatocytes in mice. In particular, TRIP13 localizes as a single
286 filament between the SC lateral elements. Therefore, TRIP13/Pch2 and HORMA domain proteins have
287 mutually exclusive localization patterns on the meiotic chromosome axes, providing an explanation for
288 the depletion of HORMA domain proteins from the synapsed chromosomes in diverse organisms.
289 The transverse filaments (TF) are essential for recruitment of Pch2 to the SC. In a budding yeast
290 Zip1 (encoding the TF component) allele with four amino acid substitutions, Pch2 is absent from the SC
291 (Subramanian et al., 2016). In *C. elegans*, the TF component SYP-1 is essential for localization of Pch-2
292 on the paired chromosomes (Deshong et al., 2014). In rice, CRC1 (Pch2 orthologue) and CEP1 (TF
293 protein) localize to the SC in an inter-dependent manner (Miao et al., 2013). In *Arabidopsis*, ZYP1 (TF
294 component) recruits Pch2 to the SC (Yang et al., 2022). In the yeast two-hybrid assay, rice CRC1
295 interacts with CEP1, *Arabidopsis* ZYP1 interacts with Pch2, and mouse SYCP1 (TF protein) interacts
296 with TRIP13 (Miao et al., 2013; Yang et al., 2022). Unlike in other species, loss of SYCP1 (TF protein) in
297 mouse leads to a complete failure in chromosomal synapsis and thus its role in recruitment of TRIP13 to
298 the synapsed SC can not be directly addressed (de Vries et al., 2005). Our findings on the localization of
299 mouse TRIP13 to the SC on the sister chromatids in *Rec8*-deficient spermatocytes and the short SC
300 stretches in *Sycp2* mutant spermatocytes demonstrate that TRIP13 recruitment is independent of SC axial
301 element proteins REC8 and SYCP2 but support the possibility that SYCP1 could recruit TRIP13 to the
302 synapsed SC. These findings lead to the following model: the TF protein recruits Pch2/TRIP13 to the SC
303 upon synapsis, which in turn evicts HORMA domain proteins from the synapsed regions (Figure 7C).
304 Both TRIP13 and SKP1 are required for removal of HORMA domain proteins from the synapsed
305 SC (Guan et al., 2020; Wojtasz et al., 2009). However, the relationship of TRIP13 and SKP1 is unknown.
306 SKP1 localizes to the synapsed SC more extensively than TRIP13. While TRIP13 is only detected on the
307 synapsed SC in early pachytene spermatocytes (Figure 1), SKP1 localizes to the synapsed SC in zygotene,
308 all stages of pachytene, and diplotene spermatocytes (Guan et al., 2020). The localization of TRIP13 and

309 SKP1 within the SC is different: TRIP13 is on CE/TF regions but SKP1 on LEs. While the global level of
310 TRIP13 is reduced in *Skp1*-deficient testes, the localization of TRIP13 and SKP1 to the synapsed SC is
311 independent (Figure 6D) (Guan et al., 2020). The SCF ubiquitin E3 ligase complex targets HORMAD1
312 for ubiquitination and degradation in transfected HEK293T cells (Guan et al., 2022). Loss of TRIP13
313 leads to accumulation of HORMAD proteins only to the synapsed SC in pachytene cells. In contrast,
314 depletion of SKP1 causes accumulation of HORMA domain proteins, particularly HORMAD1, on both
315 unsynapsed and synapsed chromosome axes from leptotene through diplotene meiocytes. Therefore,
316 TRIP13 and SKP1 might regulate different pools of HORMAD proteins in meiocytes (Figure 7C).
317 In many organisms including mouse and human, centromeres are the last regions to synapse (Bisig
318 et al., 2012; Brown et al., 2005; Qiao et al., 2012). The reason for this is unknown, but it might be related
319 to the necessity to suppress deleterious non-homologous recombination at centromere and pericentromeric
320 regions, which consist of minor and major satellite repeats respectively. The centromere was proposed to
321 exert an inhibitory effect on synapsis in human cells (Brown et al., 2005). The inhibition needs to be
322 relieved to achieve full synapsis, since unsynapsis at centromeres is expected to trigger the meiotic
323 checkpoint, leading to meiotic arrest. To date, only two mouse mutants (*Skp1* and *Trip13*) exhibit
324 unsynapsis preferentially at the centromeric end in pachytene-like cells. In addition, only these two mouse
325 mutants display abnormal accumulation of HORMAD proteins on the synapsed SC. Intriguingly, TRIP13
326 localizes to telomeres in both spermatocytes and oocytes. The centromere is close to one of the telomeres
327 in mouse. Thus, the preferential centromeric end asynapsis in *Trip13* or *Skp1*-deficient meiocytes could be
328 related to abnormal persistence of HORMAD proteins. However, the underlying molecular mechanism
329 warrants further investigation.
330 We find that TRIP13 is a dosage-dependent regulator of meiosis. The *Trip13*$^{+/-}$ mice displayed
331 reduced testis weight, reduced sperm count, and meiotic defects but these defects were less severe than
332 the *Trip13*$^{-/-}$ mice. The disease phenotypes in humans also appear to be influenced by the *TRIP13* dosage
333 (Yost et al., 2017; Zhang et al., 2020). The dosage-dependent phenotypic variation has been reported in
334 other mouse meiotic mutants such as *Tex11*, *Meiob*, and *Rnf212*. TEX11 localizes to meiotic
335 chromosomes as foci and regulates crossover formation and chromosome synapsis (Yang et al., 2008).
336 The TEX11 protein levels correlate with genome-wide recombination rates in mice (Yang et al., 2015).
337 MEIOB, a meiosis-specific ssDNA-binding protein, is essential for meiotic recombination (Luo et al.,
338 2013; Souquet et al., 2013). In mice with different combinations of *Meiob* alleles, MEIOB protein levels
339 directly correlate with the severity of meiotic defects (Guo et al., 2020). Sequence variants in human
340 RNF212 are associated with variations in genome-wide recombination rates (Chowdhury et al., 2009;
341 Kong et al., 2008). In mouse, RNF212 forms foci on meiotic chromosomes and regulates crossover

342 formation in a dosage-dependent manner (Reynolds et al., 2013). Therefore, dosage sensitivity appears to
343 be a common feature of many regulators of meiosis.
344
345 **Materials and Methods**
346
347 **Ethics statement**
348 Mice were maintained and used for experimentation according to the protocol approved by the
349 Institutional Care and Use Committee of the University of Pennsylvania.
350
351 **Mouse strains**
352 The cryopreserved sperm from *Trip13*$^{+/-}$ males were obtained from the Mutant Mouse Resource and
353 Research Center (MMRCC) at UC Davis (*Trip13*$^{tm1.1(KOMP)Vlcg/JMmucd}$, MMRRC_050223-UCD).
354 Genotyping of wild type and knockout *Trip13* alleles was performed by separate PCR reactions using tail
355 genomic DNA. Other mutant mouse lines used in this study were previously generated: *Hormad1*, *Sycp2*,
356 and *Rec8* (Guan et al., 2020; Shin et al., 2010; Yang et al., 2006). Genotyping PCR primer sequences are
357 listed in Table 2.
358
359 **Generation of 3×FLAG-*Trip13* and *Trip13*-3×FLAG knockin mouse strains**
360 The 3×FLAG-knockin mouse strains were generated by the CRISPR-Cas9 mediated genome editing
361 approach. To generate N-terminally tagged knockin mice, one single-guide RNA (sgRNA) was designed
362 to target the first exon of the mouse *Trip13* (Figure 7 – figure supplement 1A). A ssDNA repair template
363 was created using the sequence surrounding the start codon as 5′ and 3′ homology arms. The knockin
364 template itself included the sequence for the 3×FLAG epitope and a three-residue linker sequence. The C-
365 terminally tagged strain was generated similarly (Figure 7 – figure supplement 1B). The guide RNA
366 targeted exon 13 containing the stop codon. The ssDNA template contained the FLAG-encoding
367 sequences and homology sequences flanking the insertion site. sgRNA sequences and ssDNA template
368 sequences were shown in Table 2.
369 For the sgRNA, the oligo was phosphorylated, annealed, and cloned to PX330 plasmid (Addgene,
370 Waterton, MA). After *in vitro* transcription with the MEGAshortscript T7 Kit (AM1354, Invitrogen) and
371 purification with the MEGAclear Transcription Clean-Up Kit (AM1908, Invitrogen), a mixture of Cas9
372 mRNA [100ng/µl; Trilink, catalog number L-7206) + 0.5 µl of the sgRNA (35 ng/µl) + 100ng/ul of
373 ssDNA template] was prepared and injected into zygotes. The injected zygotes were cultured in KSOM
374 medium at 37°C in a 5% CO_2 incubator until the two-cell stage. The two-cell embryos were transferred

375 into oviducts of 0.5-day post-coitum pseudopregnant ICR foster mothers. Founder mice were bred to wild
376 type mice to obtain germline transmission. The N-terminal 3×FLAG allele and the C-terminal 3×FLAG
377 allele were PCR amplified and sequenced to confirm the insertion. PCR genotyping primers are listed in
378 Table 2.
379
380 **Production of anti-MAJIN antibodies**
381 The short isoform of mouse MAJIN (amino acids 1-124; XM_036161650.1 and XP_036017543.1) was
382 expressed as a 6xHis-MAJIN recombinant protein in *E. coli* using the pQE-30 vector. The recombinant
383 protein was affinity purified with the Ni-NTA agarose. Two guinea pigs were immunized at Cocalico
384 Biologicals Inc. (Reamstown, PA), resulting in two antisera (UP-GP140 and UP-GP141). Both anti-sera
385 were used for immunofluorescence of nuclear spreads of spermatocytes.
386
387 **Histological, immunofluorescence, and surface nuclear spread analyses**
388 For histology, testes or ovaries were fixed in Bouin's solution at room temperature overnight, embedded
389 with paraffin, and sectioned at 8 μm. Sections were stained with hematoxylin and eosin. For
390 immunofluorescence analysis, testes were fixed in 4% paraformaldehyde (in 1×PBS) overnight at 4°C,
391 dehydrated in 30% sucrose (in 1×PBS) overnight, and sectioned at 8 μm in a cryostat. Surface nuclear
392 spread analysis was described before (Peters et al., 1997). Briefly, testicular tubules or ovarian tissues
393 were soaked in hypotonic treatment buffer (30 mM Tris, 50 mM sucrose, 17 mM trisodium citrate
394 dihydrate, 5 mM EDTA, 0.5 mM DTT, 1 mM PMSF). Then the cells were suspended in 100 mM sucrose
395 and spread by physical disruption on "PTFE" printed slides that were previously soaked with
396 paraformaldehyde solution containing Triton X-100 and sodium borate. Antibodies used for
397 immunostaining are listed in Table 3.
398
399 **Imaging**
400 Histological images were captured on the Leica DM5500B microscope with a DFC450 digital camera
401 (Leica Microsystems, Wetzlar, Germany). Most immunolabeled chromosome spread images were taken
402 on the Leica DM5500B microscope with an ORCA Flash4.0 digital monochrome camera (Hamamatsu
403 Photonics, Bridgewater, NJ). Confocal microscopy of immunolabeled chromosome spreads was
404 performed on a Leica SP5 II confocal (Leica Microsystems, Wetzlar, Germany) with an 100× (1.46 NA)
405 oil immersion objective lens. Images were deconvolved with Huygens Essential deconvolution software
406 (Scientific Volume Imaging B.V., Hilversum, Netherlands).
407

408 ***Western blot analysis***

409 Testes were homogenized in the lysis buffer (50 mM Tris-HCl, pH 8.0, 150 mM NaCl, 1% Trion X-100,
410 0.5% sodium deoxycholate, 5 mM $MgCl_2$, and 1 mM DTT supplemented with 1 mM PMSF). 40 μg of
411 protein samples were resolved by SDS-PAGE, transferred onto PDVF membranes, and immunoblotted
412 with primary antibodies (Table 3).

413

414 **Acknowledgements**

415 We thank Gordon Ruthel at the PennVet Imaging Core for help with super-resolution microscopy, Hsin
416 Yao Tang and Thomas Beer at Wistar Proteomics Core for help with mass spectrometry, Christer Hoog
417 for SYCP1 antibody, Attila Toth for HORMAD2 antibody, Scott Keeney for anti-REC114 antibody,
418 Yoshinori Watanabe and Takashi Akera for CENP-C antibody.

419

420 **Competing interests**: The authors declare that no competing interests exist.

421

422 **Funding**

423 This work was supported by National Institutes of Health/National Institute of Child Health and Human
424 Development grants T32HD083185 (JYC), R01HD109253 (PJW), and P50HD068157 (PJW).

425

426 ## References

427 **Balboni, M., Yang, C., Komaki, S., Brun, J. and Schnittger, A.** (2020). COMET Functions as a PCH2
428 Cofactor in Regulating the HORMA Domain Protein ASY1. *Curr Biol* **30**, 4113-4127 e4116.
429 **Bisig, C. G., Guiraldelli, M. F., Kouznetsova, A., Scherthan, H., Hoog, C., Dawson, D. S. and Pezza,**
430 **R. J.** (2012). Synaptonemal complex components persist at centromeres and are required for
431 homologous centromere pairing in mouse spermatocytes. *PLoS genetics* **8**, e1002701.
432 **Boekhout, M., Karasu, M. E., Wang, J., Acquaviva, L., Pratto, F., Brick, K., Eng, D. Y., Xu, J.,**
433 **Camerini-Otero, R. D., Patel, D. J., et al.** (2019). REC114 Partner ANKRD31 Controls Number,
434 Timing, and Location of Meiotic DNA Breaks. *Molecular cell* **74**, 1053-1068.e1058.
435 **Brown, P. W., Judis, L., Chan, E. R., Schwartz, S., Seftel, A., Thomas, A. and Hassold, T. J.** (2005).
436 Meiotic synapsis proceeds from a limited number of subtelomeric sites in the human male.
437 *American Journal of Human Genetics* **77**, 556-566.
438 **Chen, C., Jomaa, A., Ortega, J. and Alani, E. E.** (2014). Pch2 is a hexameric ring ATPase that
439 remodels the chromosome axis protein Hop1. *Proceedings of the National Academy of Sciences of*
440 *the United States of America* **111**, 44.
441 **Chowdhury, R., Bois, P. R., Feingold, E., Sherman, S. L. and Cheung, V. G.** (2009). Genetic analysis
442 of variation in human meiotic recombination. *PLoS genetics* **5**, e1000648.
443 **Daniel, K., Lange, J., Hached, K., Fu, J., Anastassiadis, K., Roig, I., Cooke, H. J., Stewart, A. F.,**
444 **Wassmann, K., Jasin, M., et al.** (2011). Meiotic homologue alignment and its quality
445 surveillance are controlled by mouse HORMAD1. *Nature cell biology* **13**, 599-610.
446 **de Vries, F. A., de Boer, E., van den Bosch, M., Baarends, W. M., Ooms, M., Yuan, L., Liu, J. G.,**
447 **van Zeeland, A. A., Heyting, C. and Pastink, A.** (2005). Mouse Sycp1 functions in

448 synaptonemal complex assembly, meiotic recombination, and XY body formation. *Genes &*
449 *development* **19**, 1376-1389.
450 **Deshong, A. J., Ye, A. L., Lamelza, P. and Bhalla, N.** (2014). A quality control mechanism coordinates
451 meiotic prophase events to promote crossover assurance. *PLoS Genet* **10**, e1004291.
452 **Fukuda, T., Daniel, K., Wojtasz, L., Toth, A. and Hoog, C.** (2010). A novel mammalian HORMA
453 domain-containing protein, HORMAD1, preferentially associates with unsynapsed meiotic
454 chromosomes. *Experimental cell research* **316**, 158-171.
455 **Gomez, H. L., Felipe-Medina, N., Condezo, Y. B., Garcia-Valiente, R., Ramos, I., Suja, J. A.,**
456 **Barbero, J. L., Roig, I., Sanchez-Martin, M., de Rooij, D. G., et al.** (2019). The PSMA8
457 subunit of the spermatoproteasome is essential for proper meiotic exit and mouse fertility. *PLoS*
458 *Genet* **15**, e1008316.
459 **Guan, Y., Leu, N. A., Ma, J., Chmatal, L., Ruthel, G., Bloom, J. C., Lampson, M. A., Schimenti, J.**
460 **C., Luo, M. and Wang, P. J.** (2020). SKP1 drives the prophase I to metaphase I transition during
461 male meiosis. *Science advances* **6**, eaaz2129.
462 **Guan, Y., Lin, H., Leu, N. A., Ruthel, G., Fuchs, S. Y., Busino, L., Luo, M. and Wang, P. J.** (2022).
463 SCF ubiquitin E3 ligase regulates DNA double-strand breaks in early meiotic recombination.
464 *Nucleic Acids Res* **50**, 5129-5144.
465 **Guo, R., Xu, Y., Leu, N. A., Zhang, L., Fuchs, S. Y., Ye, L. and Wang, P. J.** (2020). The ssDNA-
466 binding protein MEIOB acts as a dosage-sensitive regulator of meiotic recombination. *Nucleic*
467 *acids research* **48**, 12219-12233.
468 **Handel, M. A. and Schimenti, J. C.** (2010). Genetics of mammalian meiosis: regulation, dynamics and
469 impact on fertility. *Nature reviews.Genetics* **11**, 124-136.
470 **Herruzo, E., Lago-Maciel, A., Baztan, S., Santos, B., Carballo, J. A. and San-Segundo, P. A.** (2021).
471 Pch2 orchestrates the meiotic recombination checkpoint from the cytoplasm. *PLoS Genet* **17**,
472 e1009560.
473 **Herruzo, E., Ontoso, D., Gonzalez-Arranz, S., Cavero, S., Lechuga, A. and San-Segundo, P. A.**
474 (2016). The Pch2 AAA+ ATPase promotes phosphorylation of the Hop1 meiotic checkpoint
475 adaptor in response to synaptonemal complex defects. *Nucleic Acids Res* **44**, 7722-7741.
476 **Hunter, N.** (2015). Meiotic Recombination: The Essence of Heredity. *Cold Spring Harbor perspectives*
477 *in biology* **7**, 10.1101/cshperspect.a016618.
478 **Joshi, N., Barot, A., Jamison, C. and Borner, G. V.** (2009). Pch2 links chromosome axis remodeling at
479 future crossover sites and crossover distribution during yeast meiosis. *PLoS Genet* **5**, e1000557.
480 **Karlseder, J., Kachatrian, L., Takai, H., Mercer, K., Hingorani, S., Jacks, T. and de Lange, T.**
481 (2003). Targeted deletion reveals an essential function for the telomere length regulator Trf1.
482 *Molecular and cellular biology* **23**, 6533-6541.
483 **Kim, J., Ishiguro, K., Nambu, A., Akiyoshi, B., Yokobayashi, S., Kagami, A., Ishiguro, T., Pendas,**
484 **A. M., Takeda, N., Sakakibara, Y., et al.** (2015). Meikin is a conserved regulator of meiosis-I-
485 specific kinetochore function. *Nature* **517**, 466-471.
486 **Kim, Y., Rosenberg, S. C., Kugel, C. L., Kostow, N., Rog, O., Davydov, V., Su, T. Y., Dernburg, A.**
487 **F. and Corbett, K. D.** (2014). The chromosome axis controls meiotic events through a
488 hierarchical assembly of HORMA domain proteins. *Dev Cell* **31**, 487-502.
489 **Klare, K., Weir, J. R., Basilico, F., Zimniak, T., Massimiliano, L., Ludwigs, N., Herzog, F. and**
490 **Musacchio, A.** (2015). CENP-C is a blueprint for constitutive centromere-associated network
491 assembly within human kinetochores. *The Journal of cell biology* **210**, 11-22.
492 **Kogo, H., Tsutsumi, M., Inagaki, H., Ohye, T., Kiyonari, H. and Kurahashi, H.** (2012a). HORMAD2
493 is essential for synapsis surveillance during meiotic prophase via the recruitment of ATR activity.
494 *Genes Cells* **17**, 897-912.
495 **Kogo, H., Tsutsumi, M., Ohye, T., Inagaki, H., Abe, T. and Kurahashi, H.** (2012b). HORMAD1-
496 dependent checkpoint/surveillance mechanism eliminates asynaptic oocytes. *Genes Cells* **17**, 439-
497 454.

498 **Kong, A., Thorleifsson, G., Stefansson, H., Masson, G., Helgason, A., Gudbjartsson, D. F.,**
499 **Jonsdottir, G. M., Gudjonsson, S. A., Sverrisson, S., Thorlacius, T., et al.** (2008). Sequence
500 variants in the RNF212 gene associate with genome-wide recombination rate. *Science (New York,*
501 *N.Y.)* **319**, 1398-1401.
502 **Kwon, M. S., Hori, T., Okada, M. and Fukagawa, T.** (2007). CENP-C is involved in chromosome
503 segregation, mitotic checkpoint function, and kinetochore assembly. *Mol Biol Cell* **18**, 2155-2168.
504 **Lambing, C., Osman, K., Nuntasoontorn, K., West, A., Higgins, J. D., Copenhaver, G. P., Yang, J.,**
505 **Armstrong, S. J., Mechtler, K., Roitinger, E., et al.** (2015). Arabidopsis PCH2 Mediates
506 Meiotic Chromosome Remodeling and Maturation of Crossovers. *PLoS Genet* **11**, e1005372.
507 **Li, X. C. and Schimenti, J. C.** (2007). Mouse pachytene checkpoint 2 (trip13) is required for completing
508 meiotic recombination but not synapsis. *PLoS genetics* **3**, e130.
509 **Long, J., Huang, C., Chen, Y., Zhang, Y., Shi, S., Wu, L., Liu, Y., Liu, C., Wu, J. and Lei, M.**
510 (2017). Telomeric TERB1-TRF1 interaction is crucial for male meiosis. *Nat Struct Mol Biol* **24**,
511 1073-1080.
512 **Luo, M., Yang, F., Leu, N. A., Landaiche, J., Handel, M. A., Benavente, R., La Salle, S. and Wang,**
513 **P. J.** (2013). MEIOB exhibits single-stranded DNA-binding and exonuclease activities and is
514 essential for meiotic recombination. *Nature communications* **4**, 2788.
515 **Luo, X., Tang, Z., Xia, G., Wassmann, K., Matsumoto, T., Rizo, J. and Yu, H.** (2004). The Mad2
516 spindle checkpoint protein has two distinct natively folded states. *Nat Struct Mol Biol* **11**, 338-345.
517 **Miao, C., Tang, D., Zhang, H., Wang, M., Li, Y., Tang, S., Yu, H., Gu, M. and Cheng, Z.** (2013).
518 Central region component1, a novel synaptonemal complex component, is essential for meiotic
519 recombination initiation in rice. *Plant Cell* **25**, 2998-3009.
520 **Pacheco, S., Marcet-Ortega, M., Lange, J., Jasin, M., Keeney, S. and Roig, I.** (2015). The ATM
521 signaling cascade promotes recombination-dependent pachytene arrest in mouse spermatocytes.
522 *PLoS genetics* **11**, e1005017.
523 **Page, S. L. and Hawley, R. S.** (2004). The genetics and molecular biology of the synaptonemal complex.
524 *Annual Review of Cell and Developmental Biology* **20**, 525-558.
525 **Papanikos, F., Clement, J. A. J., Testa, E., Ravindranathan, R., Grey, C., Dereli, I., Bondarieva, A.,**
526 **Valerio-Cabrera, S., Stanzione, M., Schleiffer, A., et al.** (2019). Mouse ANKRD31 Regulates
527 Spatiotemporal Patterning of Meiotic Recombination Initiation and Ensures Recombination
528 between X and Y Sex Chromosomes. *Mol Cell* **74**, 1069-1085 e1011.
529 **Peters, A. H., Plug, A. W., van Vugt, M. J. and de Boer, P.** (1997). A drying-down technique for the
530 spreading of mammalian meiocytes from the male and female germline. *Chromosome research :*
531 *an international journal on the molecular, supramolecular and evolutionary aspects of*
532 *chromosome biology* **5**, 66-68.
533 **Prince, J. P. and Martinez-Perez, E.** (2022). Functions and Regulation of Meiotic HORMA-Domain
534 Proteins. *Genes (Basel)* **13**.
535 **Qiao, H., Chen, J. K., Reynolds, A., Hoog, C., Paddy, M. and Hunter, N.** (2012). Interplay between
536 synaptonemal complex, homologous recombination, and centromeres during mammalian meiosis.
537 *PLoS genetics* **8**, e1002790.
538 **Raina, V. B. and Vader, G.** (2020). Homeostatic Control of Meiotic Prophase Checkpoint Function by
539 Pch2 and Hop1. *Curr Biol* **30**, 4413-4424 e4415.
540 **Reynolds, A., Qiao, H., Yang, Y., Chen, J. K., Jackson, N., Biswas, K., Holloway, J. K., Baudat, F.,**
541 **de Massy, B., Wang, J., et al.** (2013). RNF212 is a dosage-sensitive regulator of crossing-over
542 during mammalian meiosis. *Nature genetics* **45**, 269-278.
543 **Rinaldi, V. D., Bolcun-Filas, E., Kogo, H., Kurahashi, H. and Schimenti, J. C.** (2017). The DNA
544 Damage Checkpoint Eliminates Mouse Oocytes with Chromosome Synapsis Failure. *Mol Cell* **67**,
545 1026-1036 e1022.
546 **Roeder, G. S. and Bailis, J. M.** (2000). The pachytene checkpoint. *Trends in genetics : TIG; Trends in*
547 *genetics : TIG* **16**, 395-403.

548 **Roig, I., Dowdle, J. A., Toth, A., de Rooij, D. G., Jasin, M. and Keeney, S.** (2010). Mouse
549 TRIP13/PCH2 is required for recombination and normal higher-order chromosome structure
550 during meiosis. *PLoS genetics* **6**, 10.1371/journal.pgen.1001062.
551 **Russo, A. E., Giacopazzi, S., Deshong, A., Menon, M., Ortiz, V., Ego, K. M., Corbett, K. D. and**
552 **Bhalla, N.** (2023). The conserved AAA ATPase PCH-2 distributes its regulation of meiotic
553 prophase events through multiple meiotic HORMADs in C. elegans. *PLoS Genet* **19**, e1010708.
554 **San-Segundo, P. A. and Roeder, G. S.** (1999). Pch2 links chromatin silencing to meiotic checkpoint
555 control. *Cell* **97**, 313-324.
556 **Shibuya, H., Hernandez-Hernandez, A., Morimoto, A., Negishi, L., Hoog, C. and Watanabe, Y.**
557 (2015). MAJIN Links Telomeric DNA to the Nuclear Membrane by Exchanging Telomere Cap.
558 *Cell* **163**, 1252-1266.
559 **Shibuya, H., Ishiguro, K. and Watanabe, Y.** (2014). The TRF1-binding protein TERB1 promotes
560 chromosome movement and telomere rigidity in meiosis. *Nature cell biology* **16**, 145-156.
561 **Shin, Y. H., Choi, Y., Erdin, S. U., Yatsenko, S. A., Kloc, M., Yang, F., Wang, P. J., Meistrich, M. L.**
562 **and Rajkovic, A.** (2010). Hormad1 mutation disrupts synaptonemal complex formation,
563 recombination, and chromosome segregation in mammalian meiosis. *PLoS genetics* **6**, e1001190.
564 **Sironi, L., Mapelli, M., Knapp, S., De Antoni, A., Jeang, K. T. and Musacchio, A.** (2002). Crystal
565 structure of the tetrameric Mad1-Mad2 core complex: implications of a 'safety belt' binding
566 mechanism for the spindle checkpoint. *EMBO J* **21**, 2496-2506.
567 **Souquet, B., Abby, E., Herve, R., Finsterbusch, F., Tourpin, S., Le Bouffant, R., Duquenne, C.,**
568 **Messiaen, S., Martini, E., Bernardino-Sgherri, J., et al.** (2013). MEIOB Targets Single-Strand
569 DNA and Is Necessary for Meiotic Recombination. *PLoS genetics* **9**, e1003784.
570 **Stanzione, M., Baumann, M., Papanikos, F., Dereli, I., Lange, J., Ramlal, A., Trankner, D.,**
571 **Shibuya, H., de Massy, B., Watanabe, Y., et al.** (2016). Meiotic DNA break formation requires
572 the unsynapsed chromosome axis-binding protein IHO1 (CCDC36) in mice. *Nature cell biology*
573 **18**, 1208-1220.
574 **Subramanian, V. V., MacQueen, A. J., Vader, G., Shinohara, M., Sanchez, A., Borde, V.,**
575 **Shinohara, A. and Hochwagen, A.** (2016). Chromosome Synapsis Alleviates Mek1-Dependent
576 Suppression of Meiotic DNA Repair. *PLoS Biol* **14**, e1002369.
577 **West, A. M., Rosenberg, S. C., Ur, S. N., Lehmer, M. K., Ye, Q., Hagemann, G., Caballero, I., Uson,**
578 **I., MacQueen, A. J., Herzog, F., et al.** (2019). A conserved filamentous assembly underlies the
579 structure of the meiotic chromosome axis. *Elife* **8**.
580 **West, A. M. V., Komives, E. A. and Corbett, K. D.** (2018). Conformational dynamics of the Hop1
581 HORMA domain reveal a common mechanism with the spindle checkpoint protein Mad2. *Nucleic*
582 *Acids Res* **46**, 279-292.
583 **Wojtasz, L., Cloutier, J. M., Baumann, M., Daniel, K., Varga, J., Fu, J., Anastassiadis, K., Stewart,**
584 **A. F., Reményi, A., Turner, J. M., et al.** (2012). Meiotic DNA double-strand breaks and
585 chromosome asynapsis in mice are monitored by distinct HORMAD2-independent and -dependent
586 mechanisms. *Genes Dev* **26**, 958-973.
587 **Wojtasz, L., Daniel, K., Roig, I., Bolcun-Filas, E., Xu, H., Boonsanay, V., Eckmann, C. R., Cooke,**
588 **H. J., Jasin, M., Keeney, S., et al.** (2009). Mouse HORMAD1 and HORMAD2, two conserved
589 meiotic chromosomal proteins, are depleted from synapsed chromosome axes with the help of
590 TRIP13 AAA-ATPase. *PLoS genetics* **5**, e1000702.
591 **Xu, H., Beasley, M. D., Warren, W. D., van der Horst, G. T. and McKay, M. J.** (2005). Absence of
592 mouse REC8 cohesin promotes synapsis of sister chromatids in meiosis. *Developmental cell* **8**,
593 949-961.
594 **Xu, H., Tong, Z., Ye, Q., Sun, T., Hong, Z., Zhang, L., Bortnick, A., Cho, S., Beuzer, P., Axelrod, J.,**
595 **et al.** (2019). Molecular organization of mammalian meiotic chromosome axis revealed by
596 expansion STORM microscopy. *Proc Natl Acad Sci U S A* **116**, 18423-18428.

597 **Yang, C., Hu, B., Portheine, S. M., Chuenban, P. and Schnittger, A.** (2020). State changes of the
598 HORMA protein ASY1 are mediated by an interplay between its closure motif and PCH2. *Nucleic*
599 *Acids Res* **48**, 11521-11535.
600 **Yang, C., Sofroni, K., Hamamura, Y., Hu, B., Elbasi, H. T., Balboni, M., Chu, L., Stang, D., Heese,**
601 **M. and Schnittger, A.** (2022). ZYP1-mediated recruitment of PCH2 to the synaptonemal
602 complex remodels the chromosome axis leading to crossover restriction. *Nucleic Acids Res* **50**,
603 12924-12937.
604 **Yang, F., De La Fuente, R., Leu, N. A., Baumann, C., McLaughlin, K. J. and Wang, P. J.** (2006).
605 Mouse SYCP2 is required for synaptonemal complex assembly and chromosomal synapsis during
606 male meiosis. *The Journal of cell biology* **173**, 497-507.
607 **Yang, F., Gell, K., van der Heijden, G. W., Eckardt, S., Leu, N. A., Page, D. C., Benavente, R., Her,**
608 **C., Hoog, C., McLaughlin, K. J., et al.** (2008). Meiotic failure in male mice lacking an X-linked
609 factor. *Genes & development* **22**, 682-691.
610 **Yang, F., Silber, S., Leu, N. A., Oates, R. D., Marszalek, J. D., Skaletsky, H., Brown, L. G., Rozen,**
611 **S., Page, D. C. and Wang, P. J.** (2015). TEX11 is mutated in infertile men with azoospermia and
612 regulates genome-wide recombination rates in mouse. *EMBO molecular medicine* **7**, 1198-1210.
613 **Ye, Q., Kim, D. H., Dereli, I., Rosenberg, S. C., Hagemann, G., Herzog, F., Toth, A., Cleveland, D.**
614 **W. and Corbett, K. D.** (2017). The AAA+ ATPase TRIP13 remodels HORMA domains through
615 N-terminal engagement and unfolding. *EMBO J* **36**, 2419-2434.
616 **Yost, S., de Wolf, B., Hanks, S., Zachariou, A., Marcozzi, C., Clarke, M., de Voer, R., Etemad, B.,**
617 **Uijttewaal, E., Ramsay, E., et al.** (2017). Biallelic TRIP13 mutations predispose to Wilms tumor
618 and chromosome missegregation. *Nat Genet* **49**, 1148-1151.
619 **Zhang, Z., Li, B., Fu, J., Li, R., Diao, F., Li, C., Chen, B., Du, J., Zhou, Z., Mu, J., et al.** (2020). Bi-
620 allelic Missense Pathogenic Variants in TRIP13 Cause Female Infertility Characterized by Oocyte
621 Maturation Arrest. *American Journal of Human Genetics* **107**, 15-23.
622 **Zickler, D. and Kleckner, N.** (2015). Recombination, Pairing, and Synapsis of Homologs during
623 Meiosis. *Cold Spring Harbor perspectives in biology* **7**, 10.1101/cshperspect.a016626.
624

625

626 **Figure Legends**

627

628 **Figure 1.** TRIP13 localizes to the synaptonemal complex and telomeres in spermatocytes. (A) Western
629 blot analysis of TRIP13 in adult mouse tissues. Heart and skeletal muscle lack ACTB. (B)
630 Immunofluorescence of TRIP13 in sections of 3-month-old wild type and *Trip13*$^{-/-}$ testes. Lep, leptotene;
631 Zyg, zygotene; Pac, pachytene; eS, elongating spermatids; ES, elongated spermatids. (C)
632 Immunofluorescence of TRIP13 in spread nuclei of spermatocytes from wild type P20 testes. (D) Super-
633 resolution localization of TRIP13 to the central element (CE) but not lateral element (LE) of the
634 synaptonemal complex at early pachytene stage. The enlarged view of the boxed chromosome is shown at
635 the bottom.

636

637 **Figure 2.** Loss of *Trip13* leads to meiotic arrest in males. (A) Image of testes from 2 to 3 month-old mice.
638 (B) Western blot analysis of TRIP13 in P21 testes. SYCP3 serves as a meiosis-specific marker. ACTB
639 serves as a loading control. (C) Testis to body weight ratio of 2 to 3 month-old mice. n = 3 males.
640 Statistics, one-Way ANOVA. (D) Sperm count of 2 to 3 month-old *Trip13*$^{+/+}$ and *Trip13*$^{+/-}$ males. n = 3
641 males. Statistics, one-Way ANOVA. (E) Histological analysis of 2-month-old testes. Sertoli, Sertoli cell;
642 Zyg, zygotene; Pa-like, pachytene-like; Dip, diplotene; eS, elongating spermatids.

643

644 **Figure 3.** *Trip13* is required for chromosomal synapsis in males. (A) Composition of prophase I
645 spermatocytes in P20 testes. Three males per genotype were analyzed by nuclear spread analysis. Total
646 number of spermatocytes counted: *Trip13*$^{+/+}$, 1038 cells; *Trip13*$^{+/-}$, 803 cells; *Trip13*$^{-/-}$, 406 cells. (B)
647 Immunofluorescence of SYCP1 and SYCP3 in spread nuclei of pachytene spermatocytes from P20 testes.
648 (C) Immunofluorescence of SYCE1 and SYCP3 in spread nuclei of pachytene spermatocytes from P20
649 testes. (D) Super-resolution confocal microscopy of a *Trip13*$^{-/-}$ spermatocyte from P20 testis.
650 Immunostaining was performed for SYCP1 and SYCP3. Arrowheads indicate end asynapsis. Arrow
651 indicates interstitial asynapsis. (E) Percentage of early pachytene cells from P19-20 testes with asynapsed
652 chromosomes across three genotypes. (F) Number of homologous chromosomes with end asynapsis per
653 cell in P19-20 testes. (G) Percentage of early pachytene cells from P20 testes with asynapsed XY
654 chromosomes per mouse. The *p* values are indicated in graphs. Statistics (E-G), one-way ANOVA.

655

656 **Figure 4.** Normal localization of centromere and telomere markers in *Trip13*-deficient spermatocytes
657 from juvenile mice. (A-D) Immunofluorescent analysis of centromere and telomere markers in *Trip13*$^{+/+}$

658 and *Trip13*$^{-/-}$ pachytene spermatocytes: CREST (A), CENPC (B), TRF1 (C), and MAJIN (D). SYCP3
659 labels the lateral elements of the synaptonemal complex. Scale bars, 10 µm.
660
661 **Figure 5.** HORMAD1 and HORMAD2 accumulate on the lateral elements of synapsed autosomes in
662 *Trip13*$^{-/-}$ spermatocytes from juvenile (P19-21) mice. (A, B) Immunofluorescence of HORMAD1 (A) and
663 HORMAD2 (B) in pachytene spermatocytes. (C, D) Super-resolution imaging of HORMAD1 and
664 HORMAD2 in zygotene and pachytene spermatocytes. Enlarged views of the boxed chromosomes are
665 shown below. Scale bars: 10 µm (A, B), 5 µm (C, D).
666
667 **Figure 6.** Localization of TRIP13 to the SC is independent of individual axial element components. (A)
668 Immunofluorescent analysis of TRIP13 in *Hormad1*$^{-/-}$ spermatocytes from 2-month-old mice. (B)
669 Immunofluorescent analysis of TRIP13 in *Rec8*$^{-/-}$ spermatocytes from 2-month -old mice. (C)
670 Immunofluorescent analysis of TRIP13 in *Sycp2*$^{-/-}$ spermatocytes from 2-month -old mice. (D)
671 Immunofluorescent analysis of TRIP13 in *Skp1*^{cKO} spermatocytes from 2-month -old mice. Scale bars, 10
672 µm.
673
674 **Figure 7.** FLAG-tagged TRIP13 proteins localize correctly and are functional. (A) Western blot analysis
675 of tagged and untagged TRIP13 proteins in testes from P20 wild type (no tag), heterozygous tagged, and
676 homozygous tagged males. (B) Immunofluorescence of FLAG-tagged TRIP13 in pachytene
677 spermatocytes from P20 homozygous testes. N-terminal tag, 3×FLAG-*Trip13*; C-terminal tag, *Trip13*-
678 3×FLAG. Scale bar, 10 µm. (C) A schematic illustration of TRIP13, SKP1, HORMAD1/2, and the
679 synaptonemal complex. Relative locations of TRIP13 and SKP1 within the SC are depicted.
680 HORAMD1/2 are retained in synapsed regions in *Trip13*-decifient or *Skp1*-deficient spermatocytes.
681
682 **Figure 1 - figure supplement 1.** Immunofluorescent analysis of TRIP13 in spread nuclei of oocytes from
683 embryonic day 16.5 (E16.5) and E18.5 female embryos. Scale bars, 10 µm.
684
685 **Figure 2 - figure supplement 1.** Histological analysis of ovaries from adult (8-week) wild type and
686 *Trip13*$^{-/-}$ females. Scale bars, 200 µm.
687
688 **Figure 4 - figure supplement 1.** Immunofluorescent analysis of REC114 in spread nuclei of
689 spermatocytes from P28 wild type (*Trip13*$^{+/+}$) and *Trip13*$^{-/-}$ testes. Wild type, early pachytene; *Trip13*$^{-/-}$,
690 pachytene-like. REC114 foci are indicated by arrows. Scale bar, 10 µm.

691

692 **Figure 7 - figure supplement 1.** Generation of two *Trip13* FLAG tagged mouse lines. (A) Illustration of
693 the *Trip13* gene structure with the 3×FLAG tag at the N terminus. The guide RNA sequence is underlined
694 in green. The single strand DNA (ssDNA) oligo template (200 nt) contains the 3×FLAG-encoding
695 sequence. The PAM site is underlined in purple. One base in the PAM site is mutated in the ssDNA oligo
696 template to prevent cutting of the template strand (in purple). The position of 3×FLAG in-frame insertion
697 is designated (^) and occurs just after the endogenous start codon. Filled bars, coding regions; Open bars,
698 5′ or 3′ UTRs. (B) Illustration of the *Trip13* gene structure with the 3×FLAG tag at the C terminus. The
699 PAM cut site and guide RNA were on the reverse strand, but for clarity, the forward strand sequence is
700 shown. The 3×FLAG was inserted just before the endogenous stop codon.

701

702

703
704
705
706 **Table 1**. **List of proteins from testis identified by co-immunoprecipitation and mass spectrometry**.
707

Protein	Number of peptides in anti-FLAG IP			M.W. (kD)
	3×FLAG-TRIP13 testis	TRIP13-3×FLAG testis	Wild type testis	
TRIP13	28	36	4	51
HORMAD2	21	10	7	39
DDX46	32	6	0	117
PUF60	24	14	0	59
RBM25	19	3	2	100
RBM39	20	10	1	59
U2AF1	11	4	1	28
U2AF2	15	9	3	54
SRSF11	9	4	0	53
SPATA5	26	27	7	97
AP3D1	17	6	2	135
PRPF40A	16	3	0	108
UGP2	15	3	0	57

708
709
710
711
712

713
714
715 **Table 2. Sequences of genotyping PCR primers, sgRNA, and ssDNA templates**

Genotyping primers			
Allele	Forward	Reverse	product (bp)
Trip13 WT	GCCCTTAGCCAAGGTGGAT	TCCTTGCACCCCTAATTGAC	645
Trip13 KO	ACTTGCTTTAAAAAACCTCCCACA	CAGAAAGCAACTGCTCCCTTCTAGC	731
Sycp2 WT	AGATGAGGGCATATCACCGA	TAAGCACACTCACCATCTCC	400
Sycp2 KO	GCATGTTATCAACCTTATCCCT	CCTACCGGTGGATGTGGAATGTGTG	300
Rec8 WT	AGCAGAGTCGAAGAAGGCCTCTTG	CAGATGGTGGCGAAGCAGCCTGT	426
Rec8 KO	AGCAGAGTCGAAGAAGGCCTCTTG	TTGCTCAGGGGAATTTGGGTC	212
Hormad1 WT	TCAAGACCAACCTGGGCTAC	CCATGTGGGTTGTAGGGAGT	196
Hormad1 KO	TCAAGACCAACCTGGGCTAC	GGGGAACTTCCTGACTAGGG	~400
3×FLAG-*Trip13*	CCTACATCGGAGAAGGCTGT	TTCATGTCAGGCTGTTCAGG	WT:348 KI:426
Trip13-3×FLAG	GCCCCACTAAAGCACAAGTC	ACAGGCTTGAGTCAGGATGG	WT:405 KI:471

Genome editing		
	guide RNA	HDR ssDNA
3×FLAG-*Trip13*	ATTCCCTCGGCTCCCGGCGG	TCGGAGAAGGCTGTCGCACAGGGCGCAGGGAGGCGA CCGCGGCCTCACTCCGGCGGCATTCCCTCGGCTCCCG GCGGCAGCGCCATGGGTGACTACAAAGACCATGACG GTGATTATAAAGATCATGACATCGATTACAAGGATGA CGATGACAAGGGAAGCGGAGACGAGGCGGTGGGCGA CCTGAAGCAAGCGCTTCC
Trip13-3×FLAG	AAGCCATAGATATGGATGTC	AGGGTTTCCTCCAGGCCCTATCTCTGGCAGTGGACAA ACAGTTTGAGGAGAAAAAGAAACTTTCAGCTTATGTT GACTACAAAGACCATGACGGTGATTATAAAGATCATG ACATCGATTACAAGGATGACGATGACAAGTGATCCAA GACATCCATATCTATGGCTTTCAATGGACAAGTAGGA GGTGATACCGTCTAC

716
717

718

719

720 **Table 3. List of primary antibodies**

Reagent	Dilution	Source	Catalog # or reference
Mouse anti-ACTB mab	1:2000	Sigma	Cat# A5441; RRID: AB_476744
Human anti-centromere (CREST)	1:500	Antibodies Incorporated	Cat# 15-234; RRID: AB_2687472
Rabbit anti-SYCP1	1:300	Abcam	Cat# ab15090; RRID: AB_301636
Guinea pig anti-SYCP2	1:150	Custom made	(Yang et al., 2006)
Mouse anti-SYCP3 mab	1:500	Abcam	Cat# ab97672; RRID: AB_10678841
Rabbit anti-SYCP3	1:500 IF; 1:2000 WB	ProteinTech Group	Cat# 23024-1-AP; RRID: AB_11232426
Rabbit anti-HORMAD1	1:300	ProteinTech Group	Cat# 13917-1-AP; RRID: AB_2120844
Rabbit anti-HORMAD2	1:500	Custom made, a gift from Toth lab	(Wojtasz et al., 2009)
Rabbit anti-REC114	1:100	Custom made, a gift from Keeney Lab	(Boekhout et al., 2019)
Rabbit anti-REC8	1:200	Custom made, a gift ftom Mengcheng Luo lab	N/A
Mouse anti-FLAG mab	1:300IF; 1:4000WB	Sigma	Cat# F3165, RRID: AB_259529
Rabbit anti-SKP1	1:200 IF; 1:1000 WB	Cell Signaling	Cat# 12248S, RRID: AB_2754993
Rabbit anti-TRIP13	1:150 IF; 1:1000 WB	ProteinTech Group	19602-1-AP
Rabbit anti-SYCE1	1:200 IF; 1:1000 WB	Custom made	N/A
Mouse anti-SYCP1 mab	1:200 IF: 1:1000 WB	Custom made, 1:200; a gift from Chritster Hoog lab	N/A
Rabbit anti-CENP-C	1:500	Custom made, a gift from Y. Watanabe	(Kim et al., 2015)
Mouse anti-TRF1 mab	1:100	Sigma	T1948
Guinea pig anti- MAJIN	1:100	Custom made; this study	N/A

721

722

723

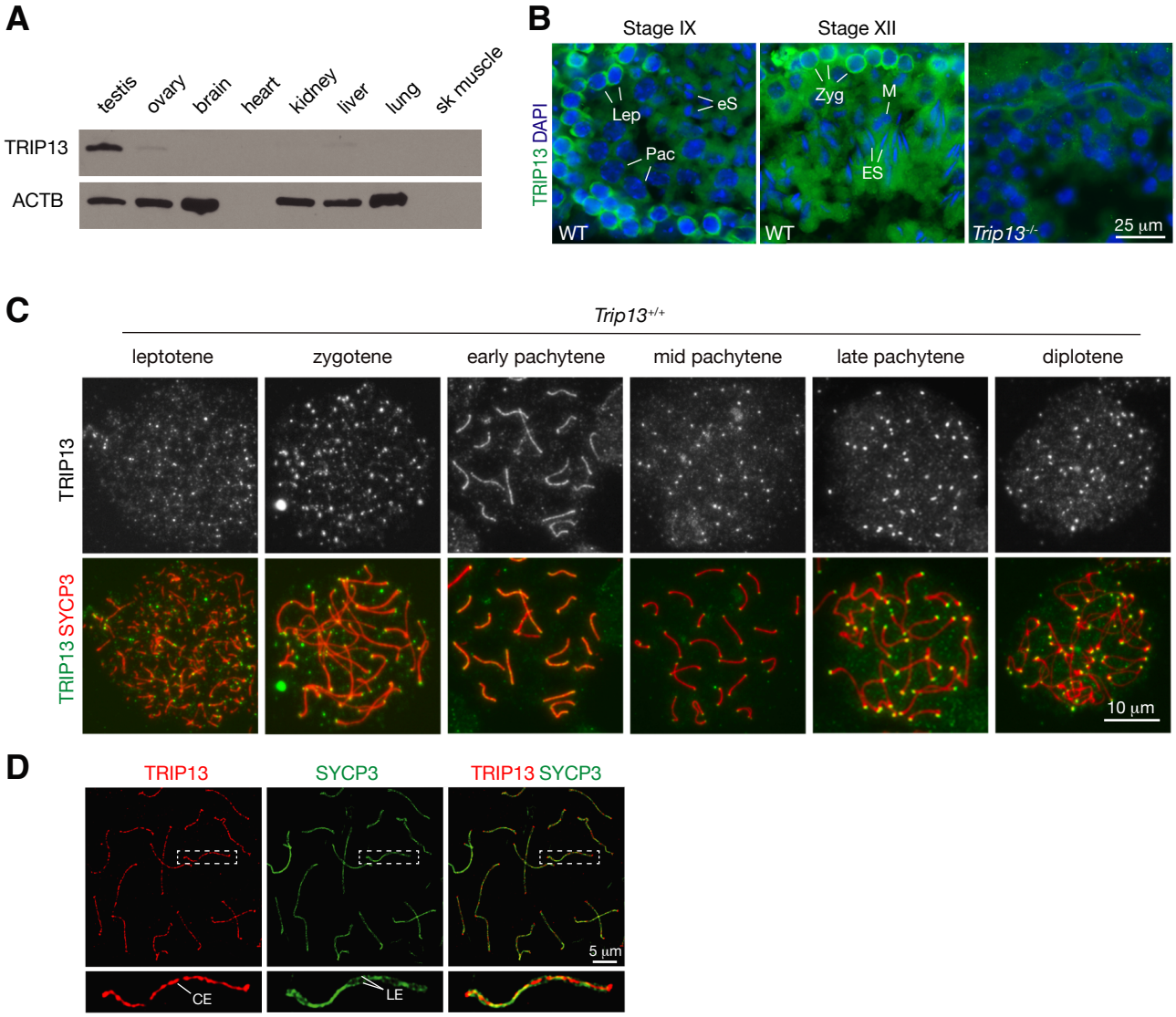
A
testis
ovary
brain
heart
kidney
liver
lung
sk muscle
TRIP13
ACTB
B
Stage IX
Stage XII
TRIP13 DAPI
Lep
eS
Pac
Zyg
M
ES
WT
WT
Trip13-/-
25 µm
C
Trip13+/+
leptotene
zygotene
early pachytene
mid pachytene
late pachytene
diplotene
TRIP13
TRIP13 SYCP3
10 µm
D
TRIP13
SYCP3
TRIP13 SYCP3
5 µm
CE
LE

Figure 1

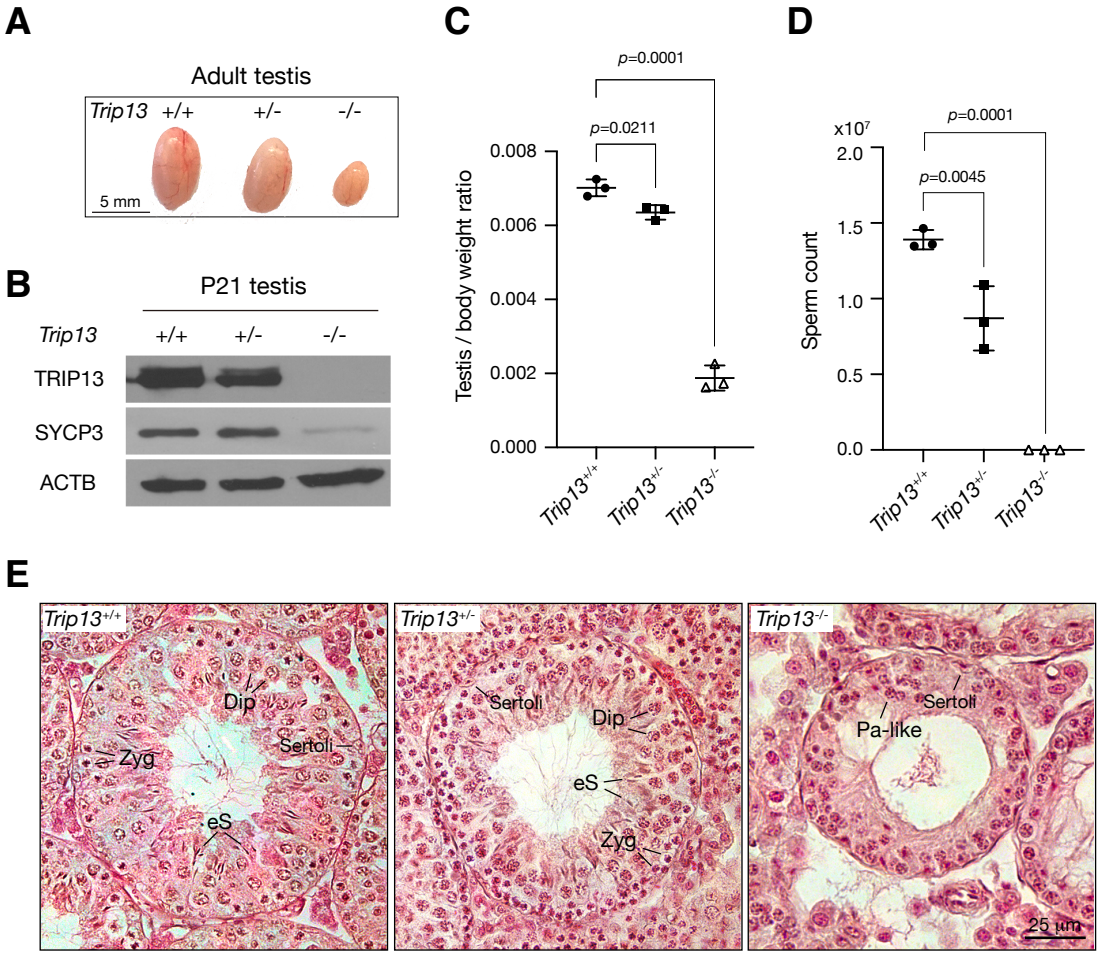
A
Adult testis
Trip13 +/+ +/- -/-
5 mm
B
P21 testis
Trip13 +/+ +/- -/-
TRIP13
SYCP3
ACTB
C
p=0.0001
p=0.0211
Testis / body weight ratio
0.008
0.006
0.004
0.002
0.000
Trip13+/+
Trip13+/-
Trip13-/-
D
x10^7
p=0.0001
p=0.0045
Sperm count
2.0
1.5
1.0
0.5
0.0
Trip13+/+
Trip13+/-
Trip13-/-
E
Trip13+/+
Dip
Sertoli
Zyg
eS
Trip13+/-
Sertoli
Dip
eS
Zyg
Trip13-/-
Sertoli
Pa-like
25 µm

Figure 2

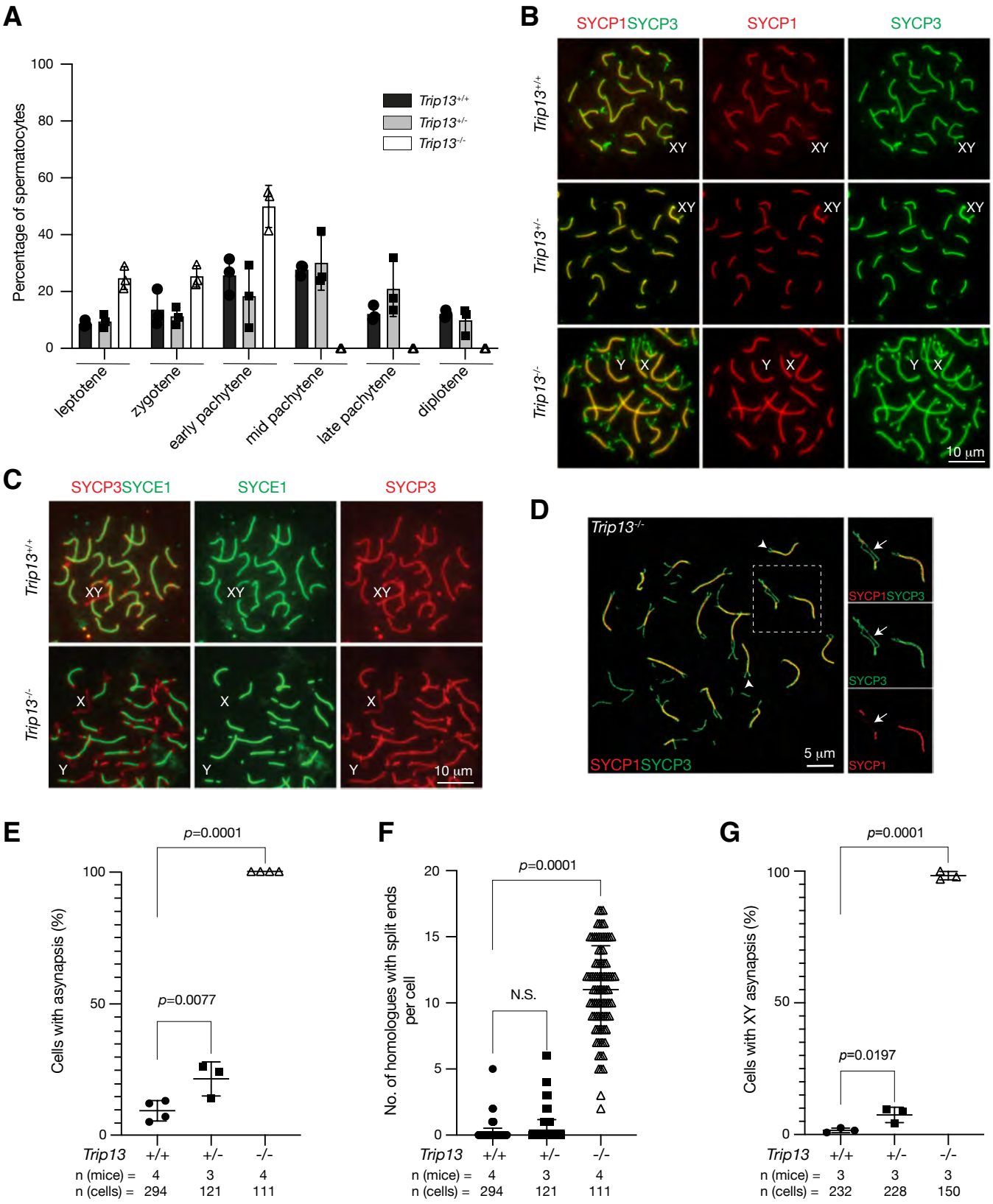
A
Percentage of spermatocytes
100
80
60
40
20
0
Trip13+/+
Trip13+/-
Trip13-/-
leptotene
zygotene
early pachytene
mid pachytene
late pachytene
diplotene
B
SYCP1SYCP3
SYCP1
SYCP3
Trip13+/+
Trip13+/-
Trip13-/-
XY
Y X
10 µm
C
SYCP3SYCE1
SYCE1
SYCP3
Trip13+/+
Trip13-/-
XY
X
Y
10 µm
D
Trip13-/-
SYCP1SYCP3
SYCP3
SYCP1
5 µm
E
p=0.0001
p=0.0077
Cells with asynapsis (%)
100
50
0
Trip13 +/+ +/- -/-
n (mice) = 4 3 4
n (cells) = 294 121 111
F
p=0.0001
N.S.
No. of homologues with split ends per cell
20
15
10
5
0
Trip13 +/+ +/- -/-
n (mice) = 4 3 4
n (cells) = 294 121 111
G
p=0.0001
p=0.0197
Cells with XY asynapsis (%)
100
50
0
Trip13 +/+ +/- -/-
n (mice) = 3 3 3
n (cells) = 232 228 150

Figure 3

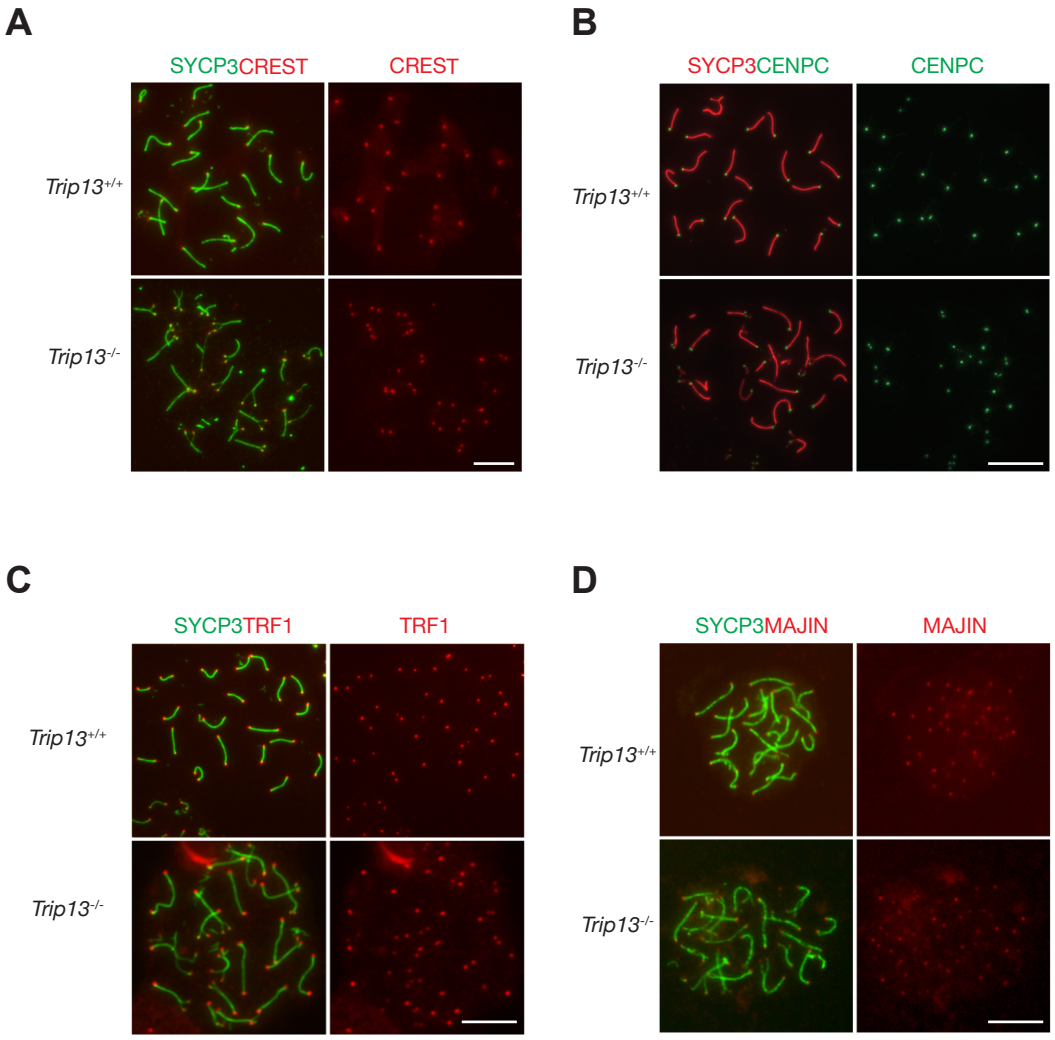
A
SYCP3CREST
CREST
Trip13+/+
Trip13-/-
B
SYCP3CENPC
CENPC
Trip13+/+
Trip13-/-
C
SYCP3TRF1
TRF1
Trip13+/+
Trip13-/-
D
SYCP3MAJIN
MAJIN
Trip13+/+
Trip13-/-

Figure 4

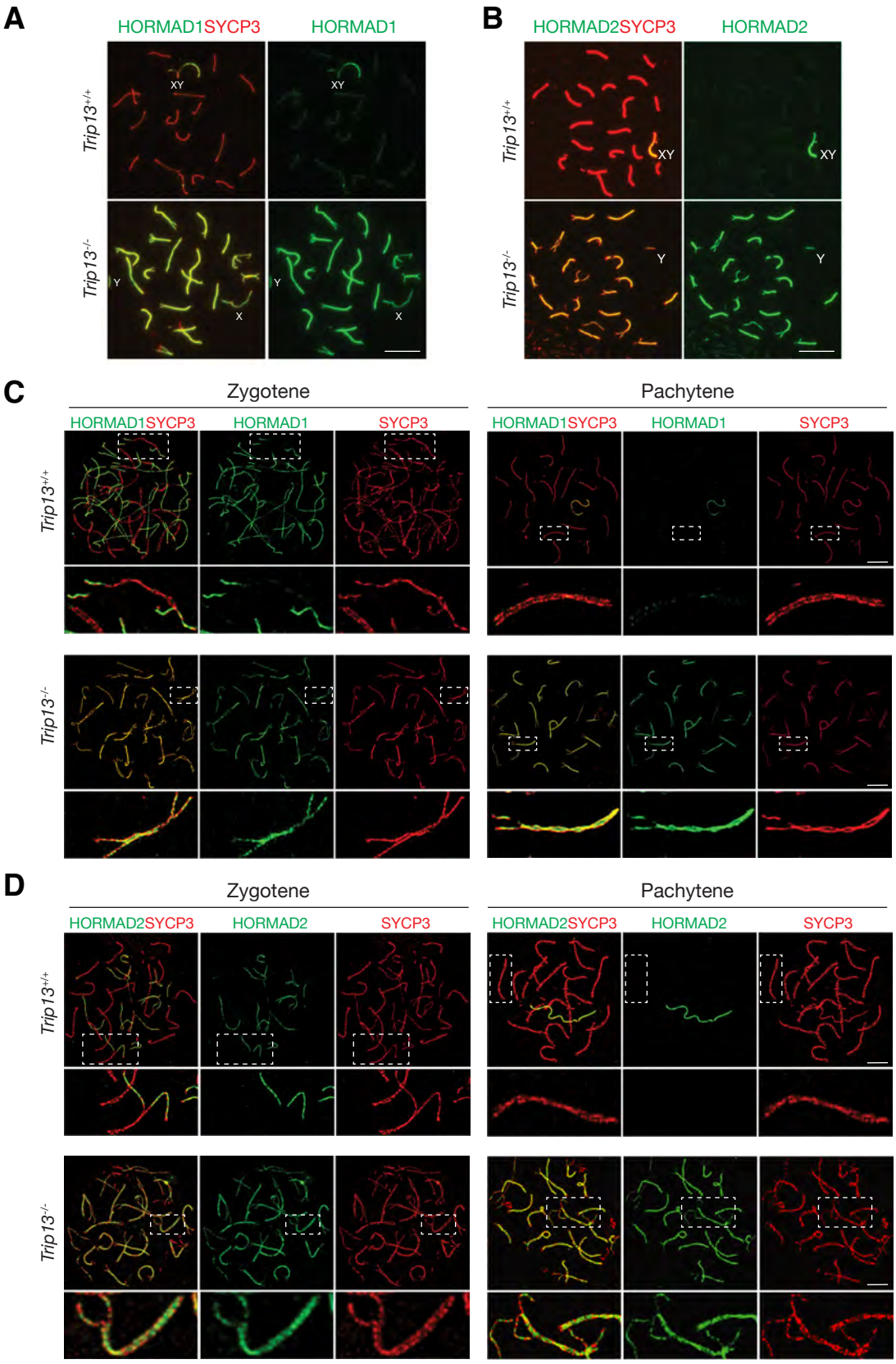
A
HORMAD1SYCP3
HORMAD1
Trip13+/+
Trip13-/-
XY
Y
X
B
HORMAD2SYCP3
HORMAD2
C
Zygotene
Pachytene
HORMAD1SYCP3
HORMAD1
SYCP3
D

Figure 5

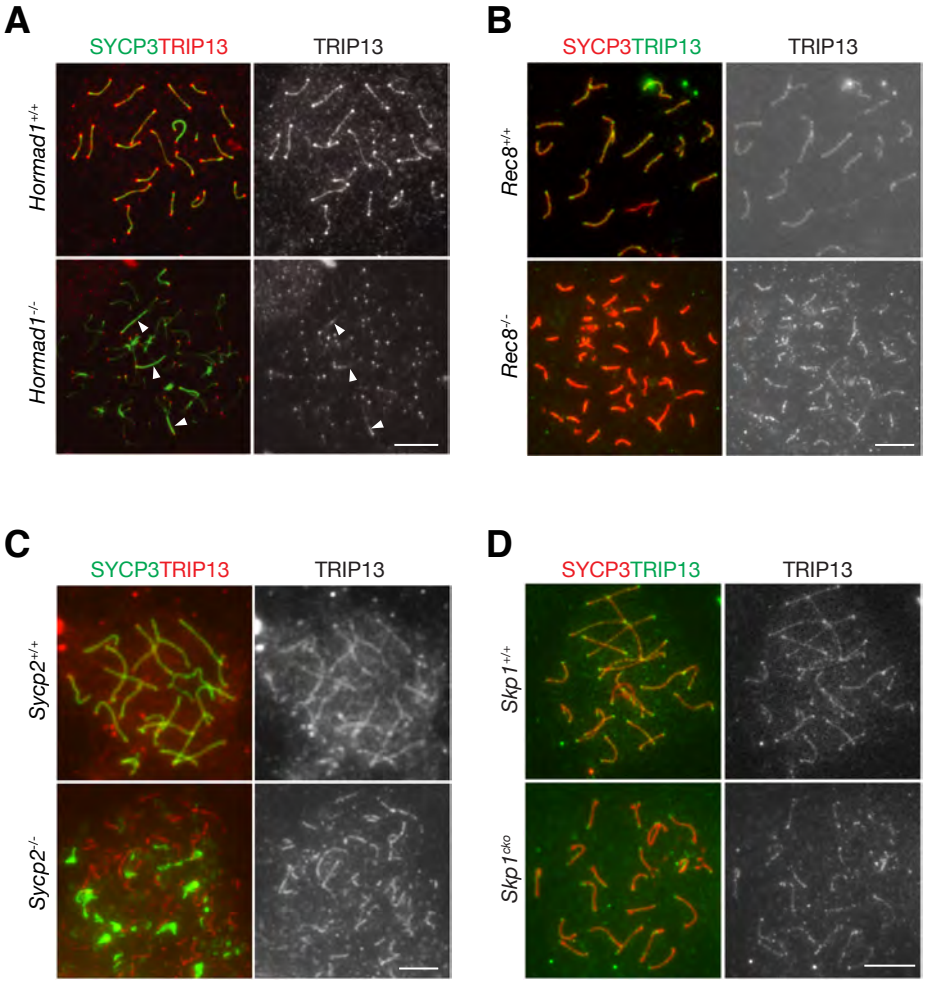
A
SYCP3TRIP13
TRIP13
Hormad1+/+
Hormad1-/-
B
SYCP3TRIP13
TRIP13
Rec8+/+
Rec8-/-
C
SYCP3TRIP13
TRIP13
Sycp2+/+
Sycp2-/-
D
SYCP3TRIP13
TRIP13
Skp1+/+
Skp1cko

Figure 6

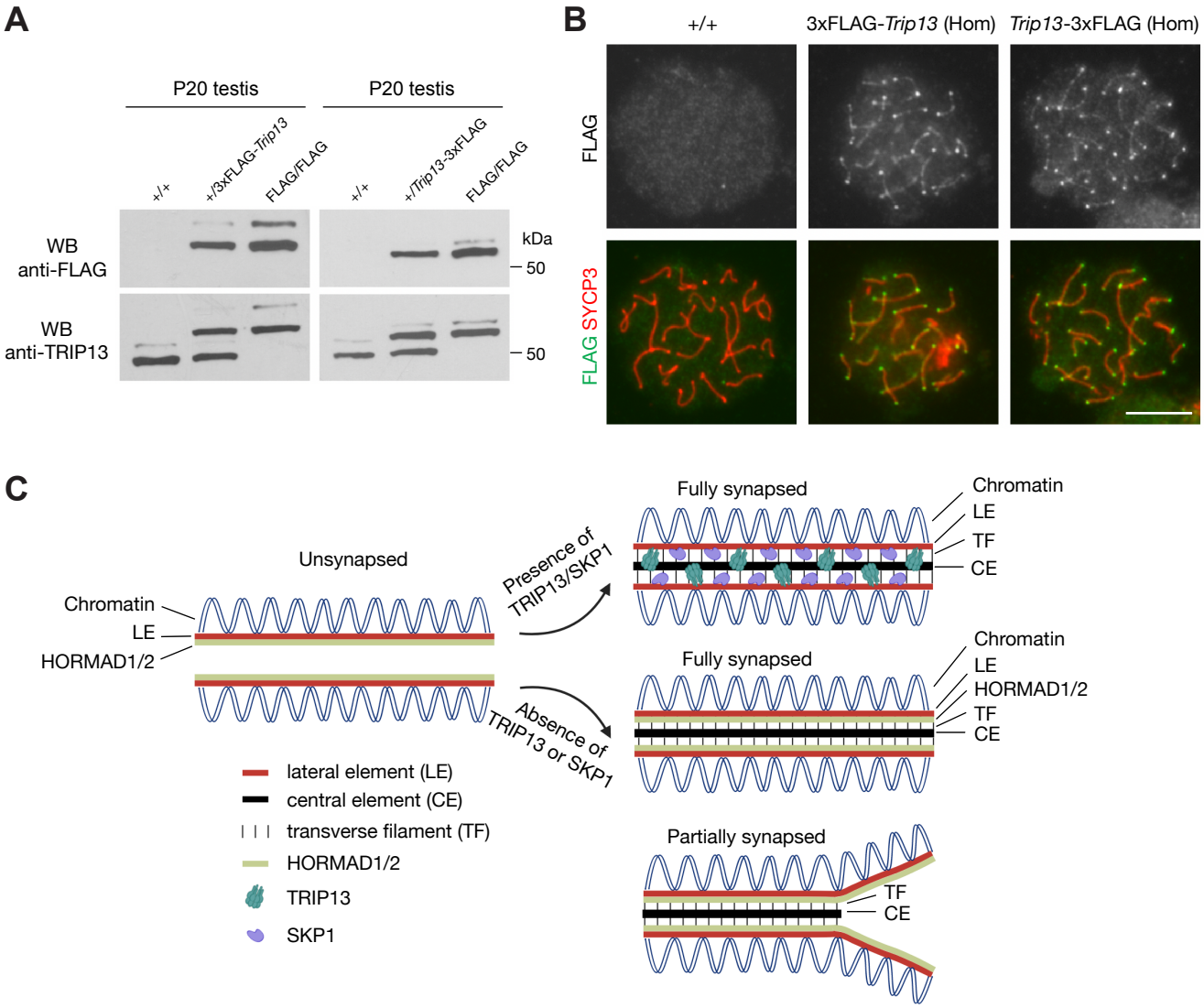
A
P20 testis
P20 testis
+/+
+/3xFLAG-Trip13
FLAG/FLAG
+/+
+/Trip13-3xFLAG
FLAG/FLAG
WB
anti-FLAG
WB
anti-TRIP13
kDa
50
50
B
+/+
3xFLAG-Trip13 (Hom)
Trip13-3xFLAG (Hom)
FLAG
FLAG SYCP3
C
Unsynapsed
Chromatin
LE
HORMAD1/2
Presence of TRIP13/SKP1
Absence of TRIP13 or SKP1
Fully synapsed
Chromatin
LE
TF
CE
Fully synapsed
Chromatin
LE
HORMAD1/2
TF
CE
Partially synapsed
TF
CE
lateral element (LE)
central element (CE)
transverse filament (TF)
HORMAD1/2
TRIP13
SKP1

Figure 7

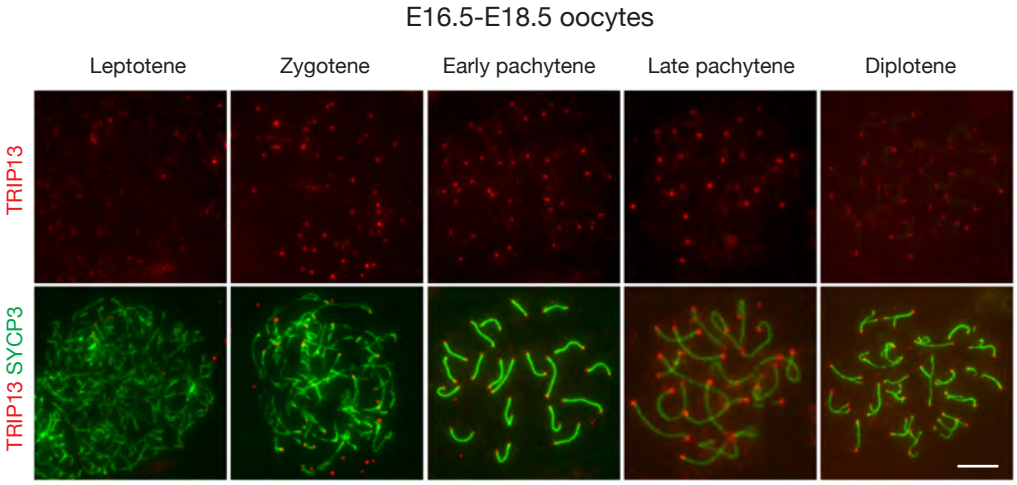

Figure 1 - supplement 1

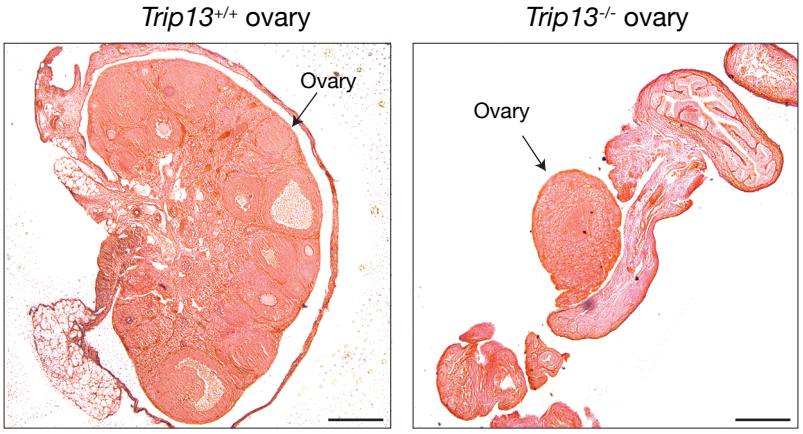

Figure 2 - supplement 1

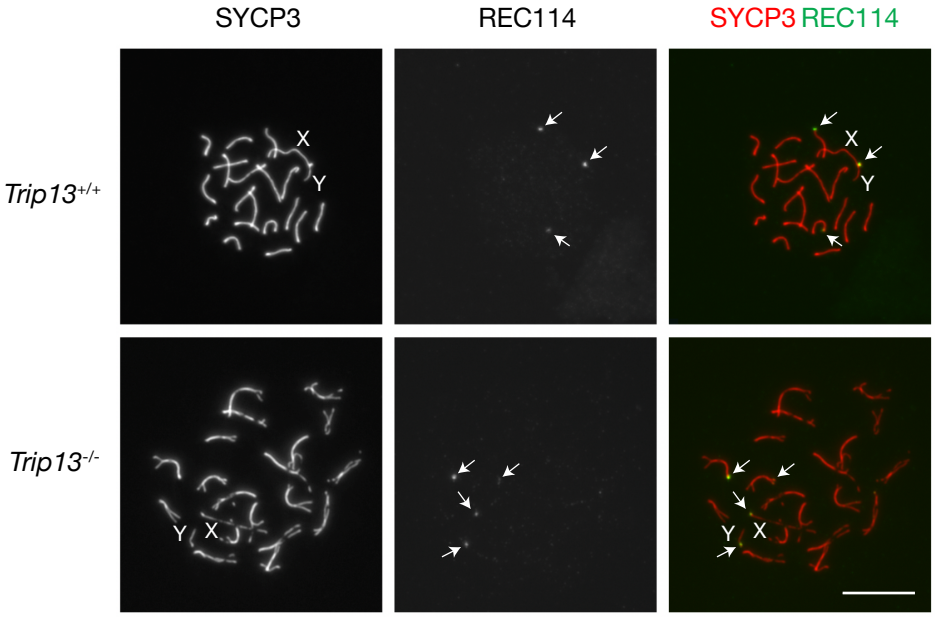

Figure 4 - figure supplement 1

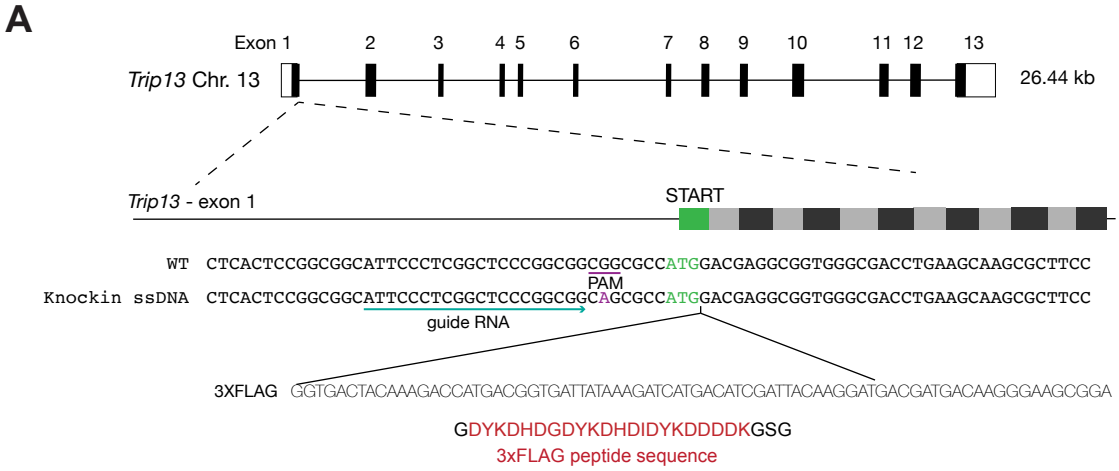

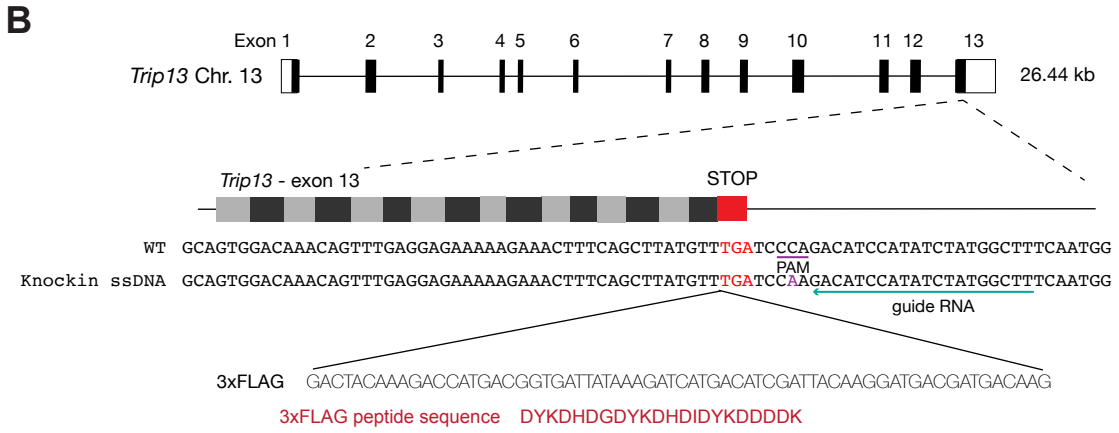

Figure 7 - supplement 1